Bayesian Learning Aided Parameter Estimation and Joint Beamformer Design in mmWave MIMO-OFDM ISAC Systems

Awadhesh Gupta, *Student Member, IEEE*, Jitendra Singh, *Student Member, IEEE*, Suraj Srivastava, *Member, IEEE*, Aditya K. Jagannatham, *Senior Member, IEEE*, Lajos Hanzo, *Life Fellow, IEEE*

***Abstract*—A three-dimensional (3D) sparse signal recovery problem formulation is conceived for delay, Doppler, and angular (DDA) domain target parameter estimation in millimeter wave (mmWave) multiple-input multiple-output (MIMO) orthogonal frequency division multiplexing (OFDM)-based integrated sensing and communication (ISAC) systems relying on a hybrid beamforming architecture. Subsequently, a 3D-sparse Bayesian learning (3D-BL) algorithm is proposed to jointly estimate the angular, range, velocity, and radar cross-section (RCS) parameters of the targets. Furthermore, an uplink beamformer is designed for the user equipment (UE) to alleviate the complexity of uplink parameter estimation at the dual-functional radar-communication (DFRC) base station (BS) by eliminating the need for angle of departure (AoD) estimation. Additionally, a Bayesian alternating minimization (BAT-MIN) algorithm is constructed for the designing of a DFRC waveform, enabling the simultaneous generation of beams toward both the radar targets and the UE. Furthermore, the sparse Bayesian learning lower bound (SBL-LB) and the Bayesian Cramér-Rao lower bound (BCRLB) are derived to serve as benchmarks for estimation performance. Finally, simulation results are presented to showcase the enhanced performance of the proposed methodologies in terms of multiple performance metrics when contrasted both to the existing sparse recovery techniques and to conventional non-sparse parameter estimation algorithms. The simulation outcomes unequivocally demonstrate the commendable performance of the proposed 3D-BL estimation methodology, approaching closely to the SBL-LB. Notably, this approach exhibits a substantial gain of at least 5 dB when compared to alternative techniques. Additionally, the introduced BAT-MIN beamformer emerges as a highly competitive solution, closely approximating the capabilities of a fully digital beamformer while maintaining a noteworthy minimum advantage over its contemporaries. These findings underscore the significance and efficacy of the proposed techniques in the context of advanced signal processing and beamforming.**

***Index Terms*—Integrated sensing and communication (ISAC), hybrid analog-digital (HAD) beamforming, dual-functional radar-communication (DFRC), sparse Bayesian learning (SBL), millimeter wave (mmWave).**

I. Introduction

The convergence of radar and communication technologies has emerged as a transformative trend that holds tremendous promise across a wide spectrum of applications. This convergence, commonly referred to as integrated sensing and communication (ISAC), represents a paradigm shift that brings traditionally distinct fields together to create synergies, unlock new capabilities and address pressing challenges [1]–[3]. The fundamental concept of ISAC involves consolidating both sensing and communication functions within a single hardware platform and utilizing joint spectral resources for both purposes [4], [5]. Compared to independent communication and radar systems, ISAC provides benefits in terms of cost, power consumption, latency and spectrum efficiency [6]. This amalgamation has opened various applications like vehicle-to-vehicle (V2V), vehicle-to-infrastructure (V2I) paradigms, indoor positioning using WiFi, and drones acting as base stations [7]–[9]. However, high communication throughput, enhanced sensing resolution, and low latency are necessary for an ISAC system to fulfill the needs of these next-generation applications.

Exploring the millimeter wave (mmWave) spectrum might be a way to overcome this challenge in next-generation (NG) systems [10], [11]. The mmWave band provides very high bandwidth, which in turn results in good range resolution in radar applications. Moreover, owing to the limited availability of multiple paths within the mmWave spectrum, radar echoes are likely to encounter reduced clutter compared to the sub-6 GHz frequency bands [12]. However, mmWave communication also has several drawbacks, including significant path loss, susceptibility to blockages and reliance on line-of-sight (LoS) propagation [13]. To elaborate further, owing to the short wavelength of mmWave signals, which allows us to reduce the inter-antenna spacing, and construct compact multiple-input multiple-output (MIMO) transmit precoding for high gain. This mitigates the path-loss problem by creating highly directional beams [14]. Furthermore, transmitting multiple data streams through spatial multiplexing is capable of enhancing the spectral efficiency. However, implementing a transceiver employing digital beamforming and a radio frequency (RF) chain for each antenna element at high-frequency mmWave

L. Hanzo would like to acknowledge the financial support of the Engineering and Physical Sciences Research Council (EPSRC) projects under grant EP/Y026721/1, EP/W032635/1, EP/Y037243/1 and EP/X04047X/1 as well as of the European Research Council's Advanced Fellow Grant QuantCom (Grant No. 789028). The work of Aditya K. Jagannatham was supported in part by the Qualcomm Innovation Fellowship; in part by the Qualcomm 6G UR Gift; and in part by the Arun Kumar Chair Professorship. The work of S. Srivastava was supported in part by IIT Jodhpur's Research Grant No. I/RIG/SUS/20240043; in part by Anusandhan National Research Foundation's PM-ECRG/2024/478/ENS; and in part by Telecom Technology Development Fund (TTDF) under Grant TTDF/6G/368. S. Srivastava and A. K. Jagannatham jointly acknowledge the funding support provided to ICON-project by DST and UKRI-EPSRC under India-UK Joint opportunity in Telecommunications Research.

Awadhesh Gupta, Jitendra Singh and Aditya K. Jagannatham are with the Department of Electrical Engineering, Indian Institute of Technology Kanpur, Kanpur 208016, India (e-mail: awadheshg20@iitk.ac.in; jitend@iitk.ac.in; adityaj@iitk.ac.in).

Suraj Srivastava is with the Department of Electrical Engineering, Indian Institute of Technology Jodhpur, Jodhpur, Rajasthan, India (e-mail: surajsri@iitj.ac.in).

Lajos Hanzo is with the School of Electronics and Computer Science, University of Southampton, Southampton SO17 1BJ, U.K. (email:lh@ecs.soton.ac.uk).

settings is demanding regarding cost, power consumption and overall complexity. To surmount this challenge and facilitate the practical implementation of mmWave MIMO dual-functional radar communication (DFRC) transceivers, one can leverage hybrid analog-digital (HAD) signal processing architectures. These architectures require a significantly lower number of RF chains compared to the conventional fully-digital (FD) architecture, [15]. In the HAD architecture, the RF transmit precoding (TPC) and receive combining (RC) operations occur at the RF front-end of the transceiver, involving a network of phase shifters that enhances directional beamforming. Furthermore, multiplexing gains are also attained through digital precoding in the baseband. As a result, the design and implementation of hybrid precoders and combiners play a crucial role in unlocking the significant performance benefits offered by mmWave MIMO technology.

In modern communication standards, orthogonal frequency division multiplexing (OFDM) is a pivotal technology, playing a vital role in 4G and 5G wireless networks. OFDM, when combined with MIMO systems, significantly augments the capacity and reliability of wireless communication networks. This enhancement is attributed to OFDM's innate resistance to multipath distortion and inter-symbol interference (ISI) as well as to its ease of synchronization and equalization. Remarkably, OFDM signals have demonstrated their versatility also in radar applications [16]. The orthogonal nature of OFDM waveforms, achieved through the fast Fourier transform (FFT) operations at the transceivers, streamlines signal processing for communication and radar sensing tasks. Consequently, the attributes of OFDM waveforms render them eminently suitable for ISAC applications [17]–[20]. Radar tasks like range-velocity (RV) estimation and target recognition often employ sparse recovery techniques due to the occurrence of sparse channels in radar applications. Therefore, sophisticated sparse recovery techniques are the need of the hour. In this context, the Bayesian learning (BL) framework has garnered significant interest in addressing sparse recovery challenges. In sparse recovery problems, the objective function of BL, based on a log-likelihood formulation exhibits a reduced number of local maxima compared to similar approaches, such as FOCUSS [21]. The Expectation-Maximization (EM) algorithm, known for its well-established characteristics, ensures global convergence for the sparse BL method. This implies that each iteration is guaranteed to decrease the cost function progressively until a stable fixed point is attained. Therefore, the robust convergence exhibited by the EM algorithm, coupled with the characteristics of the SBL-based log-likelihood, contributes to an enhanced performance in the context of sparse parameter estimation. Despite being a technique with roots harking back over a decade, BL continues to be a powerful tool for sparse recovery, demonstrating its enduring relevance and effectiveness in the NG wireless communication systems [22]–[24]. The following subsection provides a concise overview of the current state-of-the-art.

A. Review of existing works

The treatises [25], [26] considered the family of OFDM-based ISAC systems. Liyanaarachchi *et al.* in [25] proposed a maximum-likelihood (ML) framework for the estimation of the delay and Doppler parameters in an OFDM-ISAC system. Moreover, to find the optimal radar subcarrier allocation, CRLBs of the delay and Doppler estimates were optimized therein. Vargas *et al.* [26] address a challenging scenario, where the overlapped radar and communication signals, as well as the channels, are unknown to the receiver. A seminal scheme was proposed for this model that achieved blind estimations of the radar and communication parameters. Toward this, a dual-blind deconvolution (DBD) problem was formulated by the authors and then a so-called sum of multivariate atomic norms (SoMAN) minimization technique was proposed that leveraged the sparsity for the estimation of both the radar and communication parameters. However, it is crucial to emphasize that all the contributions mentioned above considered operation in the sub-6 GHz frequency band for ISAC systems. Therefore, they were unable to exploit the wider spectrum and other advantages of the mmWave band.

Kumari *et al.* in [27] created a vehicular radar model utilizing the IEEE 802.11ad standard for mmWave communication and radar operations at 60 GHz. Likewise, for a bistatic mmWave ISAC system, Dokhanchi *et al.* [28], contrasted the benefits of orthogonal-frequency-division-multiple-access (OFDMA) and phase-modulated-continuous-wave (PMCW) waveforms. However, a large number of power-hungry ADCs, DACs, and power amplifiers, necessitated by the assignment of an independent RF chain to each antenna prohibit the employment of a conventional FD beamforming transceiver design in mmWave MIMO systems. This has prompted researchers to investigate a hybrid analog-digital (HAD) beamforming framework for overcoming this impediment. In this context, Liu *et al.* [29] explored the HAD architecture's suitability for the ISAC systems and employed subspace techniques, including the multiple signal classification (MUSIC) algorithm, matched-filtering (MF), as well as angle and phase estimation (APES) for the radar target and wireless channel parameters. In a related study, the authors of [30] developed target parameter estimation algorithms, drawing inspiration from the MUSIC and MF methods for a mmWave MIMO-OFDM based full-duplex ISAC system. In this study, the researchers also developed TPCs and RCs to optimize the signal-to-noise ratio (SNR) for both downlink (DL) communication and radar target detection, while also tackling self-interference (SI) cancellation. Kaushik *et al.* [35], in their innovative paper, introduces a dynamic RF chain selection mechanism for HAD ISAC systems, focusing on energy efficiency under both radar and communication constraints. Their approach invokes fractional programming to handle the non-convex problem of optimizing the numbers of RF chains (RFCs) and employs an alternating minimization approach for hybrid precoder design. Huang *et al.* [31] proposed a radar-aided mmWave channel estimation algorithm using a deep-learning technique in vehicle-to-everything (V2X) multi-user uplink scenarios. However, it is important to note that previous studies in [29], [30], [35] assumed explicit knowledge of the number of targets at the DFRC base station, which is not the case in practical in real-world scenarios. Moreover, the deep-learning technique proposed in [31] is a computationally intensive and

TABLE I: Contrasting our contributions to the existing literature

Features	[25]	[26]	[27]	[28]	[29]	[30]	[31]	[32]	[33]	[34]	Proposed
OFDM	✓	✓	✓	✓		✓		✓	✓	✓	✓
MIMO	✓		✓	✓	✓	✓	✓	✓	✓	✓	✓
mmWave band			✓	✓	✓	✓	✓	✓	✓	✓	✓
Hybrid architecture					✓	✓	✓	✓			✓
AoA estimation				✓	✓	✓	✓	✓	✓	✓	✓
Range estimation	✓	✓	✓	✓	✓	✓		✓	✓	✓	✓
Velocity estimation	✓	✓	✓	✓	✓	✓		✓	✓	✓	✓
CRLB	✓		✓	✓			✓	✓			✓
Imaging	✓	✓	✓	✓	✓	✓		✓	✓	✓	✓
Sparsity		✓						S	✓	✓	✓
BL-based estimation									DE		✓
BL-based DFRC beamforming											✓
Simultaneous sparsity-based beamformer											✓

Note S: only for sensing, DE: Only for delay estimation

data-hungry technique.

It is worth noting that a limitation of the previously discussed solutions is that they do not take advantage of the inherent sparsity of the scattering environments at mmWave frequencies, where only a small number of radar targets or scatterers are present. Exploiting this sparsity can substantially improve the accuracy of target detection, target parameters and channel estimation. In this context, Zheng *et al.* [36] present a super-resolution algorithm for sparse OFDM passive radar signals, utilizing atomic norm constraints for modeling signal sparsity in the delay-Doppler plane. It employs a convex semidefinite program (SDP) to estimate the target parameters. Gao *et al.* [32] proposed an orthogonal matching pursuit with support refinement (OMP-SR) algorithm for radar sensing, which iteratively refines the angle estimates based on coarse initial estimates. In order to facilitate target speed measurement and payload data demodulation, the framework therein also incorporates techniques for the estimation and compensation of Doppler shifts. However, the OMP technique is sensitive to both the stopping threshold and to the choice of the sensing matrix, which leads to structural and convergence deficiencies. Moreover, the complexity of the atomic norm technique employed in [36] is very high. To address these constraints and to leverage the benefits of the BL framework in a multi-user MIMO-OFDMA system, Rahman *et al.* [33] introduced a fast marginalized block sparse BL algorithm (BSBL-FM) designed for one-dimensional (1-D) target parameter estimation [33]. The delay is initially estimated by the BSBL-FM algorithm, and subsequently, the remaining sensing parameters are determined by estimating the amplitudes corresponding to those delay positions. Although these 1D compressive sensing (CS) techniques exhibit significantly reduced complexity, their estimation performance remains modest [33]. Subsequently, authors of [34] explored radar sensing using one-dimensional (1D) to three-dimensional (3D) CS techniques, employing signals that are in line with 5G standards. However, it is worth noting that [34] did not consider the HAD architecture for mmWave MIMO systems and its impact on the associated waveform design.

To address the limitations and knowledge gaps in the prior research, we develop novel algorithms for target sensing and beamforming in mmWave MIMO-OFDM ISAC systems relying on the BL framework that also suitably exploits the sparsity in the delay-Doppler-angular domain. This leads to notable improvements in the accuracy of radar parameter estimation as well as target detection. Moreover, the BL framework in the joint beamformer design leads to significant spectral efficiency improvements compared to the competing state-of-the-art schemes. Table-I contrasts our contributions to those in the existing literature, which are further detailed in the next section.

B. Contributions

- This paper considers a mmWave MIMO-OFDM ISAC system relying on a hybrid analog-digital architecture and leverages the delay-Doppler and angular (DDA) domain sparsity for radar target parameter estimation.
- To facilitate precise radar target parameter estimation, a 3D sparse model is derived. Building on this, we propose a novel 3D-BL algorithm. This algorithm can simultaneously estimate critical radar parameters including radar cross section (RCS), range, velocity, and angle-of-arrival (AoA) of multiple moving targets at the DFRC base station.
- An uplink beamformer is proposed that utilizes the AoA estimated at the UE. This approach significantly reduces the complexity of uplink parameter estimation at the DFRC BS by bypassing the need for AoD estimation, which typically adds unnecessary computational burdens.
- A Bayesian alternating minimization (BAT-MIN) algorithm is proposed that incorporates the Bayesian learning framework alongside alternating minimization to jointly optimize radar and communication beamforming. The proposed BAT-MIN algorithm can also be adapted for dynamic RF chain selection in scenarios where the number of targets and scatterers is not known a priori. Furthermore, we benchmark the performance of the BAT-MIN algorithm against state-of-the-art algorithms such as simultaneous orthogonal matching pursuit (SOMP) [14] and M-FOCUSS-based beamformers, demonstrating superior accuracy.
- Moreover, the SBL lower bound (SBL-LB) is derived for the error covariance matrix corresponding to the estimated sparse RCS coefficients of the radar targets. Additionally, the Bayesian Cramér-Rao lower bound (BCRLB)

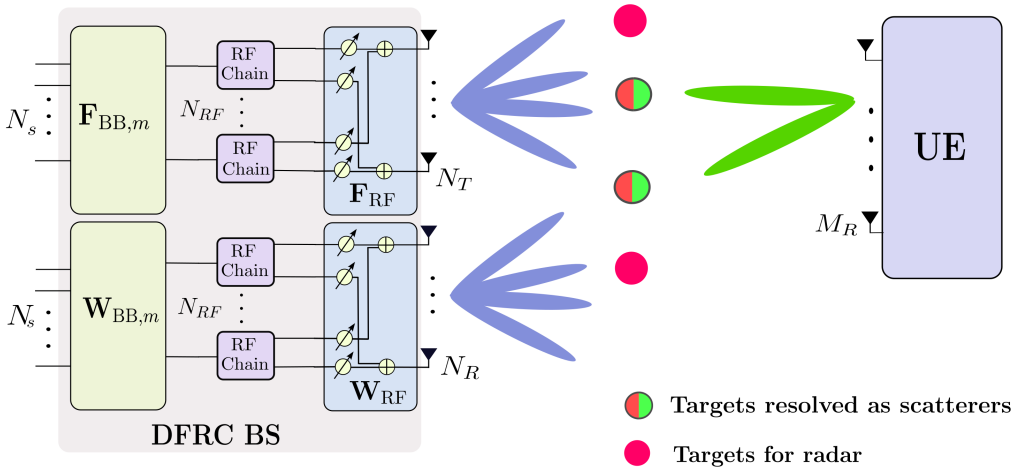

Fig. 1: mmWave MIMO-OFDM ISAC system

is derived to benchmark the NMSE performance, assuming perfect knowledge of all unknown parameters except RCS.
- Comprehensive simulation results are provided for characterizing target parameter estimation, spectral efficiency (SE) at the UE, 2D-imaging, and beampattern.

Notation: Vectors and matrices are denoted by bold lowercase and bold uppercase letters, respectively. The ith row and jth column of matrix $\mathbf{B}$ are denoted by $\mathbf{B}(i,:)$ and $\mathbf{B}(:,j)$. The operator $\mathrm{diag}(\cdot)$ extracts diagonal elements into a vector. The Kronecker product is denoted by $\otimes$. The operators $(\cdot)^T$, $(\cdot)^H$, $(\cdot)^*$, $(\cdot)^\dagger$, and $\mathrm{Tr}(\cdot)$ represent transpose, Hermitian, complex conjugate, Moore–Penrose pseudoinverse, and trace, respectively. Norms $\|\cdot\|_2$, $\|\cdot\|_0$, and $\|\cdot\|_F$ denote the ℓ_2, ℓ_0, and Frobenius norms. Finally, $\mathbb{E}\{\cdot\}$ denotes expectation.

C. Organization

This paper is organized as follows: Section-II presents a comprehensive overview of the radar and communication system models. Section-III introduces the proposed 3D-sparse radar parameter estimation framework. Section-IV describes the downlink AoA estimation and uplink beamformer design. Section-V develops the Bayesian DFRC beamforming approach. Section-VI analyzes the computational complexity of the proposed algorithms. Section-VII provides simulation results to validate the proposed methods. Section-VIII concludes the paper. Finally, the Appendix presents the derivations of the BCRLB and SBL-LB.

II. Radar and Communication System models

Consider a monostatic mmWave MIMO-OFDM ISAC system, where a DFRC BS employs N_T transmit antennas (TAs), N_R receive antennas (RAs), N_{RF} RFCs satisfying $N_{RF} \ll \min(N_T, N_R)$ and transmits $N_s < N_{RF}$ data streams as shown in Fig. 1. Given that the antenna array size at the user equipment (UE) is usually considerably smaller than that at the base station (BS) and has limited computational complexity, we assume that the UE employs a fully digital (FD) beamforming configuration. The UE is equipped with M_R RAs.

Consider a scenario, where P targets are randomly distributed throughout the scattering environment. Among these P targets, L targets are resolved as scatterers for the communication channel between the DFRC BS and UE [29]. The parameters of all the P targets are sensed at the DFRC BS, while the AoAs of the L multipath components are sensed at the UE. Therefore, the components reflected by the L communication scatterers, which also act as targets, do not create any interference at the BS.

An ISAC system is considered to operate over a total bandwidth of B Hz. The OFDM system partitions the overall bandwidth into M subcarriers, obeying $B = M\Delta f$, where Δf represents the bandwidth of each subcarrier. To meet specific constraints on the maximum delay $\tau_{\max}$ and maximum Doppler shift $\nu_{\max}$, the subcarrier spacing Δf and the symbol duration T are selected to fulfill the following conditions: $\Delta f > \nu_{\max}, \quad T > \tau_{\max}$, with $T = 1/\Delta f$ and $T_s = T + T_{cp}$, where T_{cp} is cyclic prefix (CP) duration.

A. Radar signal model

Consider that the P targets are randomly scattered at unknown locations in a radar-scattering environment. Let $\mathbf{x}_{n,m} \in \mathbb{C}^{N_s \times 1}$ denote the signal vector transmitted by the DFRC BS at time instant n and at subcarrier index m. After combining at the DFRC BS, the received echo $\bar{\mathbf{y}}_{\text{echo}}(n,m) \in \mathbb{C}^{N_s \times 1}$ can be expressed as

$$\bar{\mathbf{y}}_{\text{echo}}(n,m) = \mathbf{W}_m^H \mathbf{H}_{n,m}^r \mathbf{F}_m \mathbf{x}_{n,m} + \mathbf{W}_m^H \mathbf{v}_{n,m}, \quad (1)$$

where $\mathbf{v}_{n,m}$ denotes a symmetric complex additive white Gaussian noise (AWGN) vector distributed as $\mathcal{CN}(\mathbf{0}, \sigma_v^2 \mathbf{I}_{N_R})$. Furthermore, the matrices $\mathbf{W}_m = \mathbf{W}_{\text{RF}}\mathbf{W}_{\text{BB},m}$, $\mathbf{F}_m = \mathbf{F}_{\text{RF}}\mathbf{F}_{\text{BB},m}$ where $\mathbf{W}_{\text{BB},m} \in \mathbb{C}^{N_{RF} \times N_s}$ and $\mathbf{F}_{\text{BB},m} \in \mathbb{C}^{N_{RF} \times N_s}$ represent the frequency selective baseband RC and TPC, respectively, corresponding to the mth subcarrier. Moreover, $\mathbf{W}_{\text{RF}} \in \mathbb{C}^{N_R \times N_{RF}}$ and $\mathbf{F}_{\text{RF}} \in \mathbb{C}^{N_T \times N_{RF}}$ are the RF RC and RF TPC, respectively. Since, the RF TPC and RC are

constructed using a digitally controlled network of the phase-shifters, $\mathbf{W}_{\text{RF}}$ and $\mathbf{F}_{\text{RF}}$ are constrained to have constant magnitude entries of $|\mathbf{W}_{\text{RF}}(i,j)| = \frac{1}{\sqrt{N_R}}$ and $|\mathbf{F}_{\text{RF}}(i,j)| = \frac{1}{\sqrt{N_T}}$ $\forall i,j$.

The MIMO-OFDM radar channel matrix $\mathbf{H}^r_{n,m} \in \mathbb{C}^{N_R \times N_T}$ can be formulated as [37], [38]

$$\mathbf{H}^r_{n,m} = \sum_{p=1}^{P} \alpha_p e^{-\text{j}2\pi m \Delta f \tau_p} e^{\text{j}2\pi n T_s \nu_p} \mathbf{a}_R(\theta_p) \mathbf{a}^H_T(\theta_p), \quad (2)$$

where the four-tuple $(\alpha_p, \tau_p, \nu_p, \theta_p)$ signifies the complex radar cross-section coefficient (RCS), delay, Doppler and AoA/AoD of the pth target. It is important to note that, in the monostatic ISAC system considered, the AoA and the AoD are the same, which is θ_p. The vectors $\mathbf{a}_R(\theta_p) \in \mathbb{C}^{N_R \times 1}$ and $\mathbf{a}_T(\theta_p) \in \mathbb{C}^{N_T \times 1}$ denote the array steering vectors at the DFRC RAs and TAs, respectively, corresponding to the AoA/AoD θ_p, which are expressed as

$$\mathbf{a}_R(\theta_p) = \left[1, e^{-\text{j}\frac{2\pi}{\lambda} d_R \sin(\theta_p)}, \ldots, e^{-\text{j}(N_R-1)\frac{2\pi}{\lambda} d_R \sin(\theta_p)}\right]^T,$$
$$\mathbf{a}_T(\theta_p) = \left[1, e^{-\text{j}\frac{2\pi}{\lambda} d_T \sin(\theta_p)}, \ldots, e^{-\text{j}(N_T-1)\frac{2\pi}{\lambda} d_T \sin(\theta_p)}\right]^T.$$

B. Downlink communication model

Assume that L multipath components exist between the DFRC BS and UE. The received signal $\bar{\mathbf{y}}_{\text{DL}}(n,m) \in \mathbb{C}^{M_R \times 1}$ at the UE can be expressed as

$$\bar{\mathbf{y}}_{\text{DL}}(n,m) = \mathbf{H}^d_{n,m} \mathbf{F}_m \mathbf{x}_{n,m} + \mathbf{z}_{n,m}, \quad (3)$$

where $\mathbf{z}_{n,m}$ is the AWGN having the distribution $\mathcal{CN}(\mathbf{0}, \sigma_z^2 \mathbf{I}_{M_R})$. Since the UE performs FD beamforming, the standard zero-forcing (ZF) or minimum mean square error (MMSE) combiner is applied for the received signal model of (3) during symbol detection. Furthermore, $\mathbf{H}^d_{n,m} \in \mathbb{C}^{M_R \times N_T}$ represents the downlink MIMO-OFDM channel's frequency response (CFR) matrix corresponding to the mth subcarrier and nth OFDM symbol, which can be expressed as [37]

$$\mathbf{H}^d_{n,m} = \sum_{\ell=1}^{L} \beta_\ell e^{-\text{j}2\pi m \Delta f \tilde{\tau}_\ell} e^{\text{j}2\pi n T_s \tilde{\nu}_\ell} \mathbf{b}_R(\phi_\ell) \mathbf{a}^H_T(\vartheta_\ell), \quad (4)$$

where $\beta_\ell, \tilde{\tau}_\ell, \tilde{\nu}_\ell, \phi_\ell$ and ϑ_ℓ denote the complex path-gain, delay, Doppler, AoA and AoD of ℓth scatterer, respectively. The vector $\mathbf{b}_R(\phi_\ell) \in \mathbb{C}^{M_R \times 1}$ represents the array steering vector at the UE, which is defined similarly as in radar signal model.

C. Uplink communication model

After combining at the DFRC BS, the received signal $\bar{\mathbf{y}}_{\text{UL}}(n,m) \in \mathbb{C}^{N_s \times 1}$ can be expressed as

$$\bar{\mathbf{y}}_{\text{UL}}(n,m) = \mathbf{W}^H_m \mathbf{H}^u_{n,m} \mathbf{U} \tilde{\mathbf{x}}_{n,m} + \mathbf{W}^H_m \tilde{\mathbf{v}}_{n,m}, \quad (5)$$

where the vector $\tilde{\mathbf{v}}_{n,m}$ is the AWGN with distribution $\mathcal{CN}(\mathbf{0}, \sigma_v^2 \mathbf{I}_{N_R})$ and $\mathbf{U} \in \mathbb{C}^{M_R \times N_s}$ denotes the precoder at the UE. The quantity $\mathbf{H}^u_{n,m} \in \mathbb{C}^{N_R \times M_T}$ represents the uplink MIMO-OFDM CFR matrix corresponding to the mth subcarrier and nth OFDM symbol, which can be expressed as

$$\mathbf{H}^u_{n,m} = \sum_{\ell=1}^{L} \beta_\ell e^{-\text{j}2\pi m \Delta f \tilde{\tau}_\ell} e^{\text{j}2\pi n T_s \tilde{\nu}_\ell} \mathbf{a}_R(\vartheta_\ell) \mathbf{b}^H_R(\phi_\ell), \quad (6)$$

where the various quantities are defined similar to (4).

III. 3D Sparse Radar parameter estimation

To construct a sparse representation of the MIMO-OFDM radar channel in the Delay-Doppler-Angle (DDA) domain, let us denote the grid sizes used for the delay, Doppler, and angular domains by G_τ, G_ν, and G_θ, respectively. Furthermore, the delay grid $\mathcal{G}(\tau)$ and Doppler grid $\mathcal{G}(\nu)$ are defined as $\mathcal{G}(\tau) = \left\{\tau_i : \tau_i = \frac{i}{M\Delta f}\right\}_{i=0}^{G_\tau - 1}$, $\mathcal{G}(\nu) = \left\{\nu_j : \nu_j = \frac{j}{NT_s}\right\}_{j=0}^{G_\nu - 1}$, respectively, and the AoA grid $\mathcal{G}(\theta)$ is defined as $\mathcal{G}(\theta) = \left\{\theta_k : \theta_k = k\frac{\pi}{G_\theta} - \frac{\pi}{2}\right\}_{k=0}^{G_\theta - 1}$. Let $\alpha_{i,j,k}$ represent the complex-valued RCS coefficient corresponding to the delay-index i, Doppler-index j and AoA-index k. The 3D-sparse radar channel model can be formulated as

$$\mathbf{H}^r_{n,m} = \sum_{i=0}^{G_\tau - 1} \sum_{j=0}^{G_\nu - 1} \sum_{k=0}^{G_\theta - 1} \alpha_{i,j,k} e^{-\text{j}2\pi \frac{m}{M} i} e^{\text{j}2\pi \frac{n}{N} j} \mathbf{a}_R(\theta_k) \mathbf{a}^H_T(\theta_k). \quad (7)$$

Then, the echo signal impinging at the DFRC receiver can be expressed as

$$\mathbf{y}_{\text{echo}}(n,m) = \mathbf{W}^H_{\text{RF}} \sum_{i,j,k} \alpha_{i,j,k} e^{-\text{j}2\pi \frac{m}{M} i} e^{\text{j}2\pi \frac{n}{N} j} \mathbf{a}_R(\theta_k) \mathbf{a}^H_T(\theta_k) \times \mathbf{F}_{\text{RF}} \mathbf{x}_{n,m} + \mathbf{W}^H_{\text{RF}} \mathbf{v}_{n,m}. \quad (8)$$

Let $\boldsymbol{\phi}_{i,j,k}(n,m) \in \mathbb{C}^{N_{RF} \times 1}$ be equivalent to

$$\boldsymbol{\phi}_{i,j,k}(n,m) = e^{-\text{j}2\pi \frac{m}{M} i} e^{\text{j}2\pi \frac{n}{N} j} \mathbf{W}^H_{\text{RF}} \mathbf{a}_R(\theta_k) \mathbf{a}^H_T(\theta_k) \mathbf{F}_{\text{RF}} \mathbf{x}_{n,m}. \quad (9)$$

The system model in (8) can be expressed as

$$\mathbf{y}_{\text{echo}}(n,m) = \sum_{i,j,k} \boldsymbol{\phi}_{i,j,k}(n,m) \alpha_{i,j,k} + \mathbf{W}^H_{\text{RF}} \mathbf{v}_{n,m}, \quad (10)$$

which can also be formulated in the more compact form of

$$\mathbf{y}_{\text{echo}}(n,m) = \widetilde{\boldsymbol{\Phi}}(n,m) \boldsymbol{\alpha} + \mathbf{W}^H_{\text{RF}} \mathbf{v}_{n,m}, \quad (11)$$

where $\widetilde{\boldsymbol{\Phi}} \in \mathbb{C}^{N_{RF} \times G_\tau G_\nu G_\theta}$ and sparse radar cross-section (RCS) vector $\boldsymbol{\alpha} \in \mathbb{C}^{G_\tau G_\nu G_\theta \times 1}$ defined as

$$\widetilde{\boldsymbol{\Phi}} = [\boldsymbol{\phi}_{0,0,0}, \boldsymbol{\phi}_{0,0,1}, \ldots, \boldsymbol{\phi}_{G_\tau - 1, G_\nu - 1, G_\theta - 1}]$$
$$\boldsymbol{\alpha} = [\boldsymbol{\alpha}_{0,0,0}, \boldsymbol{\alpha}_{0,0,1}, \ldots, \boldsymbol{\alpha}_{G_\tau - 1, G_\nu - 1, G_\theta - 1}]^T.$$

It is crucial to highlight that the vector $\boldsymbol{\alpha}$ is sparse in nature due to the fact that the number of targets obeys $P \ll G_\tau G_\nu G_\theta$. Hence, $\boldsymbol{\alpha}$ contains only a few non-zero values, which correspond to the delay, Doppler and angle tuples (i,j,k) of the targets present in the scattering environment.

The observations corresponding to M subcarriers and N_p training OFDM symbols are stacked as $\mathbf{y}_r \in \mathbb{C}^{N_{RF} M N_p \times 1}$, and defined as

$$\mathbf{y}_t = \left[\mathbf{y}^T_{echo}(0,0), \mathbf{y}^T_{echo}(0,1), \ldots, \mathbf{y}^T_{echo}(N_p - 1, M-1)\right]^T.$$

Therefore, the observation vector $\mathbf{y}_r$ can be rewritten as

$$\mathbf{y}_r = \boldsymbol{\Phi}_r \boldsymbol{\alpha} + \mathbf{v}_r, \quad (12)$$

where the quantity $\boldsymbol{\Phi}_r = \left[\widetilde{\boldsymbol{\Phi}}^T(0,0), \widetilde{\boldsymbol{\Phi}}^T(0,1), \ldots, \widetilde{\boldsymbol{\Phi}}^T(N_p - 1, M-1)\right]^T \in \mathbb{C}^{N_{RF} M N_p \times G_\tau G_\nu G_\theta}$ is the associated *dictionary matrix*. In (12) we have $\mathbf{v}_r = (\mathbf{I}_{M N_p} \otimes \mathbf{W}^H_{\text{RF}}) \tilde{\mathbf{v}}_r \in$

$\mathbb{C}^{N_{RF}MN_p\times 1}$, where the vector $\widetilde{\mathbf{v}}_r$ can be defined as $\widetilde{\mathbf{v}}_r = \left[\mathbf{v}_{0,0}^T, \mathbf{v}_{0,1}^T, \ldots, \mathbf{v}_{N_p-1,M-1}^T\right]^T$.

As this is a linear model, the optimal linear unbiased estimate of $\boldsymbol{\alpha}$ can be obtained using the popular least squares (LS) method, expressed as $\widehat{\boldsymbol{\alpha}}^{LS} = \boldsymbol{\Phi}_r^{\dagger}\mathbf{y}_r$. Moreover, the minimum mean square error (MMSE) estimate can be formulated as

$$\widehat{\boldsymbol{\alpha}}^{MMSE} = \left(\boldsymbol{\Phi}_r^H\mathbf{R}_v^{-1}\boldsymbol{\Phi}_r + \mathbf{R}_{\alpha}^{-1}\right)^{-1}\boldsymbol{\Phi}_r^H\mathbf{R}_v^{-1}\mathbf{y}_r, \tag{13}$$

where the covariance matrices obey $\mathbf{R}_{\alpha} = \mathbb{E}\left\{\boldsymbol{\alpha}\boldsymbol{\alpha}^H\right\} \in \mathbb{C}^{G_\tau G_\nu G_\theta \times G_\tau G_\nu G_\theta}$ and $\mathbf{R}_v = \sigma_v^2\left[\mathbf{I}_{MN_p}\otimes \mathbf{W}_{\text{RF}}^H\mathbf{W}_{\text{RF}}\right] \in \mathbb{C}^{N_{RF}MN_p\times N_{RF}MN_p}$. Although the system model outlined in (12) is essentially linear in nature and can be addressed using the LS and MMSE methods, these conventional techniques often yield sub-optimal results. This is primarily because the parameter vector $\boldsymbol{\alpha}$ exhibits strong sparsity, which is not exploited by traditional estimators. Therefore, the problem presented in (12) essentially boils down to a sparse recovery problem. Consequently, techniques such as the orthogonal matching pursuit (OMP) can be employed to determine the solution. Nevertheless, it is crucial to acknowledge that the efficiency of OMP critically relies on the careful selection of the threshold and the dictionary matrix. In this scenario, the Bayesian learning framework, as outlined in [21], has shown remarkable performance in the realm of sparse signal recovery. The subsequent section provides a detailed exposure of this novel framework within the context of 3D radar target parameter estimation.

A. 3D-BL based radar RCS parameter estimation

In the proposed 3D-BL framework, we initially assign a parameterized Gaussian prior to the unknown sparse RCS coefficient vector $\boldsymbol{\alpha}$ as [21]

$$p(\boldsymbol{\alpha};\boldsymbol{\Omega}) = \prod_{g=1}^{G_\tau G_\nu G_\theta}\frac{1}{\pi\omega_g}\exp\left(-\frac{|\boldsymbol{\alpha}(g)|^2}{\omega_g}\right), \tag{14}$$

where ω_g represents the hyperparameter associated with the gth component of $\boldsymbol{\alpha}$, governing its prior variance. The diagonal matrix composed of these hyperparameters is denoted as $\boldsymbol{\Omega} = \text{diag}\left(\boldsymbol{\omega}\right) \in \mathbb{R}^{G_\tau G_\nu G_\theta \times G_\tau G_\nu G_\theta}$, where $\boldsymbol{\omega} \in \mathbb{R}^{G_\tau G_\nu G_\theta \times 1}$ can be expressed as $\boldsymbol{\omega} = \left[\omega_1, \omega_2, .., \omega_{G_\tau G_\nu G_\theta}\right]^T$. The log-likelihood function $\log p(\mathbf{y}_r;\boldsymbol{\omega})$ can be formulated as

$$\log p(\mathbf{y}_r;\boldsymbol{\omega}) = -\varpi - \log|\boldsymbol{\Sigma}_{y_r}| - \mathbf{y}_r^H\boldsymbol{\Sigma}_{y_r}^{-1}\mathbf{y}_r, \tag{15}$$

where $\varpi = -N_{RF}MN_p\log(\pi)$ and $\boldsymbol{\Sigma}_{y_r} = (\boldsymbol{\Phi}_r\boldsymbol{\Omega}\boldsymbol{\Phi}_r^H + \mathbf{R}_v) \in \mathbb{C}^{N_{RF}MN_p\times N_{RF}MN_p}$. Since the hyperparameter vector is unknown in practice, the ML estimate of $\boldsymbol{\omega}$ can be obtained as follows

$$\widehat{\boldsymbol{\omega}}_{ML} = \arg\max_{\boldsymbol{\omega}\geqslant 0}\log p(\mathbf{y}_r;\boldsymbol{\omega}). \tag{16}$$

As a result of the non-concave nature of the log-likelihood function in (16), attempting a direct maximization of $\log p(\mathbf{y}_r;\boldsymbol{\omega})$ imposes mathematical intractability [21]. To address this issue, the iterative EM framework provides an appealing low-complexity strategy, ensuring convergence to local optima. In this algorithm, the initial step involves defining the complete data set as $\{\mathbf{y}_r, \boldsymbol{\alpha}\}$, where $\boldsymbol{\alpha}$ represents the latent variable. Let $\widehat{\boldsymbol{\Omega}}^{(j-1)}$ denote the estimate of $\boldsymbol{\Omega}$ obtained in the $(j-1)$st iteration. In the expectation step (E-step), the log-likelihood for the complete data is expressed as

$$\begin{aligned}\mathcal{L}\left(\boldsymbol{\Omega}|\widehat{\boldsymbol{\Omega}}^{(j-1)}\right) &= \mathbb{E}_{\boldsymbol{\alpha}|\mathbf{y}_r;\widehat{\boldsymbol{\Omega}}^{(j-1)}}\left\{\log p(\mathbf{y}_r,\boldsymbol{\alpha};\boldsymbol{\Omega})\right\},\\ &= \mathbb{E}\left\{\log\left[p\left(\boldsymbol{\alpha};\boldsymbol{\Omega}\right)\right]\right\} + \mathbb{E}\left\{\log\left[p\left(\mathbf{y}_r|\boldsymbol{\alpha}\right)\right]\right\}.\end{aligned} \tag{17}$$

To compute the expectation mentioned above, it is necessary to calculate the posterior density function of the parameter $\boldsymbol{\alpha}$, which can be obtained as

$$p\left(\boldsymbol{\alpha}|\mathbf{y}_r;\widehat{\boldsymbol{\Omega}}^{(j-1)}\right) = \mathcal{CN}\left(\widehat{\boldsymbol{\alpha}}^{(j)}, \boldsymbol{\Sigma}^{(j)}\right), \tag{18}$$

where $\widehat{\boldsymbol{\alpha}}^{(j)}$ and $\boldsymbol{\Sigma}_r^{(j)}$ are derived as

$$\begin{aligned}\widehat{\boldsymbol{\alpha}}^{(j)} &= \boldsymbol{\Sigma}_r^{(j)}\boldsymbol{\Phi}_r^H\mathbf{R}_v^{-1}\mathbf{y}_r,\\ \boldsymbol{\Sigma}_r^{(j)} &= \left(\boldsymbol{\Phi}_r^H\mathbf{R}_v^{-1}\boldsymbol{\Phi}_r + \left(\widehat{\boldsymbol{\Omega}}^{(j-1)}\right)^{-1}\right)^{-1}.\end{aligned} \tag{19}$$

Next, in the Maximization step (M-step), we aim for maximizing the log-likelihood function $\mathcal{L}\left(\boldsymbol{\Omega}|\widehat{\boldsymbol{\Omega}}^{(j-1)}\right)$ with respect to the hyperparameters $\boldsymbol{\Omega}$. It is evident from (17) that the second term, $\mathbb{E}\left\{\log\left[p\left(\mathbf{y}_r|\boldsymbol{\alpha}\right)\right]\right\}$, is independent of the hyperparameters $\boldsymbol{\Omega}$. Consequently, this term can be ignored during the maximization step. Thus, the optimization problem of estimating the hyperparameters $\boldsymbol{\Omega}$ in the jth iteration can be devised as

$$\begin{aligned}\widehat{\boldsymbol{\Omega}}^{(j)} &= \arg\max_{\boldsymbol{\Omega}}\mathbb{E}\left\{\log\left[p(\boldsymbol{\alpha};\boldsymbol{\Omega})\right]\right\},\\ &= \arg\max_{\boldsymbol{\Omega}}\sum_{g=1}^{G_\tau G_\nu G_\theta}\left(-\log\left(\pi\omega_g\right) - \frac{1}{\omega_g}\mathbb{E}_{\boldsymbol{\alpha}|\mathbf{y}_r;\widehat{\boldsymbol{\Omega}}^{(j-1)}}\left\{|\boldsymbol{\alpha}(g)|^2\right\}\right).\end{aligned}$$

Notably, the maximization of this equation concerning $\boldsymbol{\Omega}$ can be performed independently for each ω_g as

$$\widehat{\omega}_g^{(j)} = \arg\max_{\omega_g}\left(-\log\left(\pi\omega_g\right) - \frac{1}{\omega_g}\mathbb{E}_{\boldsymbol{\alpha}|\mathbf{y}_r;\widehat{\boldsymbol{\Omega}}^{(j-1)}}\left\{|\boldsymbol{\alpha}(g)|^2\right\}\right).$$

By setting the derivative with respect to ω_g to zero, the estimated value of the hyperparameter ω_g in the jth iteration can be formulated as

$$\widehat{\omega}_g^{(j)} = \mathbb{E}_{\boldsymbol{\alpha}|\mathbf{y}_r;\widehat{\boldsymbol{\Omega}}^{(j-1)}}\left\{|\boldsymbol{\alpha}(g)|^2\right\} = \boldsymbol{\Sigma}^{(j)}(g,g) + \left|\widehat{\boldsymbol{\alpha}}^{(j)}(g)\right|^2. \tag{20}$$

The E-step and M-step procedures mentioned above are iteratively carried out until one of the stopping conditions is met: either the maximum affordable number of iterations κ_1 is reached or $\left\|\widehat{\boldsymbol{\Omega}}^{(j)} - \widehat{\boldsymbol{\Omega}}^{(j-1)}\right\|_F^2$ falls below a predefined threshold ϵ_1. This stopping threshold is appropriately chosen to ensure accurate parameter estimation. Algorithm-1 outlines the steps involved in the proposed 3D-BL scheme for RCS parameter estimation. Moreover, the SBL-LB for the mean square error (MSE) of the sparse RCS estimate $\boldsymbol{\alpha}$ can be expressed as

$$\text{MSE}\left(\widehat{\boldsymbol{\alpha}}\right) \geqslant \text{Tr}\left\{\left(\boldsymbol{\Phi}_r^H\mathbf{R}_v^{-1}\boldsymbol{\Phi}_r + \boldsymbol{\Omega}^{-1}\right)^{-1}\right\}. \tag{21}$$

Algorithm 1: 3D-BL based sparse RCS estimation

Input: Observation vector $\mathbf{y}_r$, dictionary matrix $\mathbf{\Phi}_r$, noise covariance matrix $\mathbf{R}_v$ and stopping threshold ϵ_1 and maximum number of iterations κ_1

Initialization:

Hyperparameters $\widehat{\omega}_g^{(0)} = 1, \ \forall \ 1 \leqslant g \leqslant G_\tau G_\nu G_\theta$, i.e., $\widehat{\mathbf{\Omega}}^{(0)} = \mathbf{I}_{G_\tau G_\nu G_\theta}$, counter variable $j = 0$ and $\widehat{\mathbf{\Omega}}^{(-1)} = \mathbf{0}_{G_\tau G_\nu G_\theta}$.

while , $\left\| \widehat{\mathbf{\Omega}}^{(j)} - \widehat{\mathbf{\Omega}}^{(j-1)} \right\|_F^2 > \epsilon_1$ and $j < \kappa_1$ **do**

$j \leftarrow j + 1$,

E-Step:

$$\mathbf{\Sigma}_r^{(j)} = \left(\mathbf{\Phi}_r^H \mathbf{R}_v^{-1} \mathbf{\Phi}_r + \left(\widehat{\mathbf{\Omega}}^{(j-1)} \right)^{-1} \right)^{-1}$$

$$\widehat{\boldsymbol{\alpha}}^{(j)} = \mathbf{\Sigma}^{(j)} \mathbf{\Phi}_r^H \mathbf{R}_v^{-1} \mathbf{y}_r$$

M-Step: Update the hyperparameters

$$\widehat{\omega}_r^{(g)} = \mathbf{\Sigma}^{(j)}(g,g) + \left| \widehat{\boldsymbol{\alpha}}^{(j)}(g) \right|^2$$

end while

Output: $\widehat{\boldsymbol{\alpha}}$

A detailed explanation of the derivation is provided in Appendix. The next section presents the AoA estimation and the UL beamforming at the UE.

IV. AoA estimation and Uplink beamforming

An uplink beamformer is required to direct the signal toward the scatterer by utilizing the knowledge of AoA at the UE. Toward this, an uplink pilot is sent to the BS to estimate the delay, Doppler, and AoA of the moving scatterers. Considering the limited computational capability of the UE, only the AoA is estimated at the UE by exploiting the high-resolution 1D multiple signal classification (1D-MUSIC) algorithm as described next [39].

A. AoA estimation of scatterers at the UE

The downlink signal received by the UE is given as

$$\mathbf{y}_{\text{DL}}(n,m) = \mathbf{H}_{n,m}^d \mathbf{F}_{\text{RF}} \mathbf{x}_{n,m} + \mathbf{z}_{n,m}, \tag{22}$$

and its covariance matrix $\mathbf{R}_y \in \mathbb{C}^{M_R \times M_R}$ is evaluated as

$$\begin{aligned} \mathbf{R}_y &= \mathbb{E}[\mathbf{y}_{\text{DL}}(n,m)\mathbf{y}_{\text{DL}}(n,m)^H] \\ &= \mathbb{E}[\mathbf{H}_{n,m}^d \mathbf{F}_{\text{RF}} \mathbf{x}_{n,m} \mathbf{x}_{n,m}^H \mathbf{F}_{\text{RF}}^H (\mathbf{H}_{n,m}^d)^H] + \mathbb{E}[\mathbf{z}_{n,m}\mathbf{z}_{n,m}^H]. \end{aligned}$$

To this end, the sample covariance matrix $\widehat{\mathbf{R}}_y$ can be formulated as

$$\widehat{\mathbf{R}}_y = \frac{1}{MN_p} \sum_{m=0}^{M-1} \sum_{n=0}^{N_p-1} \mathbf{y}_{\text{DL}}(n,m) \mathbf{y}_{\text{DL}}^H(n,m). \tag{23}$$

Furthermore, the eigenvalue decomposition of $\widehat{\mathbf{R}}_y$ can be expressed as

$$\begin{aligned} \widehat{\mathbf{R}}_y &= \mathbf{Q}(\mathbf{\Lambda} + \sigma_v^2 \mathbf{I}_{M_R}) \mathbf{Q}^H \\ &= [\mathbf{Q}_s, \mathbf{Q}_n] \begin{bmatrix} \mathbf{\Lambda}_s & \mathbf{0} \\ \mathbf{0} & \mathbf{\Lambda}_n \end{bmatrix} \begin{bmatrix} \mathbf{Q}_s^H \\ \mathbf{Q}_n^H \end{bmatrix}, \end{aligned} \tag{24}$$

where $\mathbf{Q}_s = [\mathbf{q}_1, \mathbf{q}_2, \ldots, \mathbf{q}_L] \in \mathbb{C}^{M_R \times L}$ and $\mathbf{Q}_n = [\mathbf{q}_{L+1}, \mathbf{q}_2, \ldots, \mathbf{q}_{M_R - L}] \in \mathbb{C}^{M_R \times (M_R - L)}$ contain the basis that span the signal and noise subspaces, respectively. Finally, the MUSIC spectrum can be formulated as

$$P_{\text{MUSIC}}(\phi) = \frac{1}{\mathbf{b}_R^H(\phi) \mathbf{Q}_n \mathbf{Q}_n^H \mathbf{b}_R(\phi)}. \tag{25}$$

The angles corresponding to the top L peaks of the spectrum are selected as the estimated AoAs.

B. Uplink beamformer design and scatterer parameter estimation

In this section, we will design an uplink beamformer that reduces the receiver complexity while estimating the scatterer parameters at the BS. With this objective in mind, the uplink channel in (6) can be compactly represented as

$$\mathbf{H}_{n,m}^u = \mathbf{A}_R \mathbf{R} \mathbf{C} \mathbf{D} \mathbf{B}_R^H, \tag{26}$$

where $\mathbf{A}_R = [\mathbf{a}_R(\vartheta_1), \ldots, \mathbf{a}_R(\vartheta_L)] \in \mathbb{C}^{N_R \times L}$ and $\mathbf{B}_R = [\mathbf{b}_R(\phi_1), \ldots, \mathbf{b}_R(\phi_L)] \in \mathbb{C}^{M_R \times L}$. The matrices $\mathbf{R}, \mathbf{C}, \mathbf{D} \in \mathbb{C}^{L \times L}$ are diagonal matrices whose ℓth diagonal entries are $e^{-\text{j}2\pi m \Delta f \tilde{\tau}_\ell}$, β_ℓ and $e^{\text{j}2\pi n T_s \tilde{\nu}_\ell}$, respectively. Employing the above definitions, the uplink received signal $\mathbf{y}_{\text{UL}}(n,m)$ at the DFRC BS can be expressed as

$$\mathbf{y}_{\text{UL}}(n,m) = \mathbf{W}_{\text{RF}}^H \mathbf{A}_R \mathbf{R} \mathbf{C} \mathbf{D} \mathbf{B}_R^H \mathbf{U} \tilde{\mathbf{x}}_{n,m} + \mathbf{W}_{\text{RF}}^H \tilde{\mathbf{v}}_{n,m}. \tag{27}$$

Similar to the radar system model of (12) at the DFRC BS, the sparse model can be constructed to estimate the unknown parameters of the scatterers, which is given as

$$\begin{aligned} \mathbf{y}_{\text{UL}}(n,m) = \mathbf{W}_{\text{RF}}^H \sum_{i,j,k,l} \beta_{i,j,k,l} e^{-\text{j}2\pi \frac{m}{M} i} e^{\text{j}2\pi \frac{n}{N} j} \mathbf{a}_R(\vartheta_k) \mathbf{b}_R^H(\phi_l) \\ \times \mathbf{U} \tilde{\mathbf{x}}_{n,m} + \mathbf{W}_{\text{RF}}^H \tilde{\mathbf{v}}_{n,m}, \end{aligned} \tag{28}$$

where we have $\mathcal{G}(\phi) = \left\{ \phi_l : \phi_l = l \frac{\pi}{G_\phi} - \frac{\pi}{2} \right\}_{l=0}^{G_\phi - 1}$ and G_ϕ is the grid size for the AoDs at the UE. One can observe that, in contrast to the radar system model, the AoAs and AoDs are not the same for the communication system. Hence, the DFRC BS cannot exploit the 3D sparsity, but rather, it has to introduce an angular grid for the AoDs ϕ_l, which significantly increases the complexity at the receiver. Since the information of AoD at the DFRC BS is not required for transmit beamforming, the estimation of the AoD at the DFRC BS is redundant. At this juncture, one can harness the AoA estimated in the previous stage to reduce the overall complexity. To begin with, the zero-forcing (ZF) beamformer is expressed as

$$\mathbf{U} = \mathbf{B}_R (\mathbf{B}_R^H \mathbf{B}_R)^{-1}. \tag{29}$$

Upon employing this, the model in (27) reduces to

$$\begin{aligned} \mathbf{y}_{\text{UL}}(n,m) &= \mathbf{W}_{\text{RF}}^H \mathbf{A}_R \mathbf{R} \mathbf{A} \mathbf{D} \tilde{\mathbf{x}}_{n,m} + \mathbf{W}_{\text{RF}}^H \tilde{\mathbf{v}}_{n,m} \\ &= \mathbf{W}_{\text{RF}}^H \sum_{\ell=1}^{L} \beta_\ell e^{-\text{j}2\pi m \Delta f \tilde{\tau}_\ell} e^{\text{j}2\pi n T_s \tilde{\nu}_\ell} \mathbf{a}_R(\vartheta_\ell) \tilde{x}_{n,m} \\ &\quad + \mathbf{W}_{\text{RF}}^H \tilde{\mathbf{v}}_{n,m}, \end{aligned} \tag{30}$$

and the 4D-sparse model of (28) can be reduced to the 3D-sparse model given as

$$\mathbf{y}_{\mathrm{UL}}(n,m) = \mathbf{W}_{\mathrm{RF}}^{H} \sum_{i,j,k} \beta_{i,j,k} e^{-\mathrm{j}2\pi \frac{m}{M} i} e^{\mathrm{j}2\pi \frac{n}{N} j} \mathbf{a}_R(\vartheta_k) \tilde{x}_{n,m} + \mathbf{W}_{\mathrm{RF}}^{H} \tilde{\mathbf{v}}_{n,m}. \tag{31}$$

This is the similar to the (8), hence by following the procedure from (8) to (12) one can obtain the 3D-sparse model as

$$\mathbf{y}_c = \boldsymbol{\Psi}\boldsymbol{\beta} + \mathbf{w}_r, \tag{32}$$

where $\boldsymbol{\Psi} \in \mathbb{C}^{N_{RF} M N_p \times G_\tau G_\nu G_\vartheta}$ is the *dictionary matrix*. This is also a 3D-sparse model similar to (12). Hence, 3D-BL can be exploited to estimate the parameters of the scatterers. With these estimations, the BS can now differentiate which targets are resolved as scatterers, enabling the subsequent design of the beamformer. Moreover, the estimated Doppler can be used to compensate the Doppler before formulating the DFRC beamformer. The Doppler-compensated communication channel is given by

$$\mathbf{H}_{c,m} = \sum_{\ell=1}^{L} \beta_\ell e^{-\mathrm{j}2\pi m \Delta f \tilde{\tau}_\ell} \mathbf{b}_R(\phi_\ell) \mathbf{a}_T^{H}(\vartheta_\ell). \tag{33}$$

V. DFRC BEAMFORMER

In this section, a joint optimization framework is presented, aiming for deriving the DFRC beamformer capable of directing the beam toward both the $K = P - L$ targets and L targets resolved as scatterers. With this in mind, the DFRC activates $N_{RF} = P$ RFCs. The objective of the beamformer is to maximize the downlink data rate, which is given by

$$\mathrm{SE}[m] = \log_2 \left| \mathbf{I}_{M_{\mathrm{R}}} + \frac{1}{\sigma_v^2 N_{\mathrm{s}}} \mathbf{H}_{c,m} \mathbf{F}_{\mathrm{RF}} \mathbf{F}_{\mathrm{BB},m} \mathbf{F}_{\mathrm{BB},m}^{H} \mathbf{F}_{\mathrm{RF}}^{H} \mathbf{H}_{c,m}^{H} \right|. \tag{34}$$

Therefore, the joint radar and communication beamformer design problem is constructed as

$$\begin{aligned} \max_{\mathbf{F}_{\mathrm{RF}}, \mathbf{F}_{\mathrm{BB,m}}} & \sum_{m=1}^{M} \mathrm{SE}[m] \\ \text{s.t.} \quad & |\mathbf{F}_{\mathrm{RF}}(i,j)| = \frac{1}{\sqrt{N_T}}, \quad \|\mathbf{F}_{\mathrm{RF}} \mathbf{F}_{\mathrm{BB},m}\|_F^2 = N_s, \end{aligned} \tag{35}$$

where the first constraint represents the constant-modulus property of the elements in the analog beamformer and the second constraint restricts the total transmit power to unity. Nevertheless, the non-convex constant-modulus constraint linked to every component of the RF precoder $\mathbf{F}_{\mathrm{RF}}$ and the coupling of TPC in the second constraint make direct optimization of the aforementioned objective function difficult. One can approximate the above mutual information maximization problem by a Euclidean distance minimization problem between the optimal FD TPC and hybrid TPC [35], [40]. To this end, it is proposed to employ a weighted sum objective for the radar and communication tasks. This approach aims for breaking down the product $\mathbf{F}_{\mathrm{RF}} \mathbf{F}_{\mathrm{BB},m}$ into components that closely approximate the optimal FD TPC matrix $\mathbf{F}_{\mathrm{C},m}$ for the mth subcarrier during its communication operation, while simultaneously approaching the optimal radar TPC matrix $\mathbf{F}_{\mathrm{R}}$ for radar operations. This leads us to the joint optimization problem that combines radar and communication operations for the design of the hybrid TPCs, which can be expressed as:

$$\begin{aligned} \min_{\mathbf{F}_{\mathrm{RF}}, \mathbf{F}_{\mathrm{BB},m}, \mathbf{Q}_{\mathrm{T},m}} & \delta \left\| \mathbf{F}_{\mathrm{RF}} \mathbf{F}_{\mathrm{BB},m} - \mathbf{F}_{\mathrm{C},m} \right\|_F^2 \\ & + (1-\delta) \left\| \mathbf{F}_{\mathrm{RF}} \mathbf{F}_{\mathrm{BB},m} - \mathbf{F}_{\mathrm{R}} \mathbf{Q}_{\mathrm{T},m} \right\|_F^2 \\ \text{s.t.} \; & |\mathbf{F}_{\mathrm{RF}}(i,j)| = \frac{1}{\sqrt{N_T}}, \; \|\mathbf{F}_{\mathrm{RF}} \mathbf{F}_{\mathrm{BB},m}\|_F^2 = N_s, \; \mathbf{Q}_{\mathrm{T},m} \mathbf{Q}_{\mathrm{T},m}^{H} = \mathbf{I}_P, \end{aligned} \tag{36}$$

where $\delta \in [0,1]$ is the weighting factor used for striking a trade-off between the radar and communications tasks. The communication operation is prioritized with a high value of δ, whereas the radar functionality is given priority with its low value. The matrix $\mathbf{F}_{\mathrm{C},m} \in \mathbb{C}^{N_T \times N_s}$ is an ideal unconstrained FD communication-only beamformer obtained through the N_s largest right singular vectors corresponding to the Doppler-compensated channel $\mathbf{H}_{c,m}$ formulated in (33). Furthermore, the matrix $\mathbf{F}_{\mathrm{R}} = [\mathbf{a}(\theta_1), \mathbf{a}(\theta_2), .., \mathbf{a}(\theta_K)] \in \mathbb{C}^{N_T \times K}$ is the radar-only beamformer and $\mathbf{Q}_{\mathrm{T},m} \in \mathbb{C}^{K \times N_s}$ is a semi-unitary matrix applied for compensating the change of dimensions between $\mathbf{F}_{\mathrm{R}}$ as well as $\mathbf{F}_{\mathrm{C},m}$ and does not affect the radar beampattern.

The problem in (36) involves non-convexity of the objective function and constraints, which makes the problem difficult to solve. An efficient and iterative alternating minimization-based approach is proposed therefore to find a near-optimal solution. In this regard, the problem in (36) is decomposed into two separate sub-problems, where the first problem finds $\mathbf{Q}_{\mathrm{T},m}$ while fixing $\mathbf{F}_{\mathrm{RF}}$ and $\mathbf{F}_{\mathrm{BB},m}$, while the second problem is solved for $\mathbf{F}_{\mathrm{RF}}$ and $\mathbf{F}_{\mathrm{BB},m}$ simultaneously, while keeping $\mathbf{Q}_{\mathrm{T},m}$ fixed. By setting $\mathbf{F}_{\mathrm{RF}}$ and $\mathbf{F}_{\mathrm{BB},m}$ to fixed values, the sub-problem of optimizing the auxiliary matrix $\mathbf{Q}_{\mathrm{T},m}$ can be formulated as

$$\begin{aligned} \min_{\mathbf{Q}_{\mathrm{T},m}} & \left\| \mathbf{F}_{\mathrm{RF}} \mathbf{F}_{\mathrm{BB},m} - \mathbf{F}_{\mathrm{R}} \mathbf{Q}_{\mathrm{T},m} \right\|_F^2 \\ \text{s. t.} \; & \mathbf{Q}_{\mathrm{T},m} \mathbf{Q}_{\mathrm{T},m}^{H} = \mathbf{I}_P. \end{aligned} \tag{37}$$

The problem in (37) is a well-known orthogonal Procrustes problem (OPP), which can be solved by the SVD of the matrix $\mathbf{F}_{\mathrm{R}}^{H} \mathbf{F}_{\mathrm{RF}} \mathbf{F}_{\mathrm{BB},m}$. Let $\mathbf{U}_m \boldsymbol{\Sigma}_m \mathbf{V}_m^{H} = \mathbf{F}_{\mathrm{R}}^{H} \mathbf{F}_{\mathrm{RF}} \mathbf{F}_{\mathrm{BB},m}$ define its SVD. The solution of problem (37) is given by

$$\mathbf{Q}_{\mathrm{T},m} = \mathbf{U}_m \mathbf{I}_{K \times N_s} \mathbf{V}_m, \tag{38}$$

where $\mathbf{I}_{K \times N_s}$ is obtained by selecting the first K rows of an $N_s \times N_s$ identity matrix.

To find the optimum $\mathbf{F}_{\mathrm{BB},m}$ and $\mathbf{F}_{\mathrm{RF}}$ simultaneously, we formulate a sparse matrix reconstruction problem. In this regard, by fixing $\mathbf{Q}_{\mathrm{T},m}$, the sub-problem to compute $\mathbf{F}_{\mathrm{BB},m}$ is given as

$$\begin{aligned} \min_{\mathbf{F}_{\mathrm{RF}}, \mathbf{F}_{\mathrm{BB},m}} & \delta \left\| \mathbf{F}_{\mathrm{RF}} \mathbf{F}_{\mathrm{BB},m} - \mathbf{F}_{\mathrm{C},m} \right\|_F^2 \\ & + (1-\delta) \left\| \mathbf{F}_{\mathrm{RF}} \mathbf{F}_{\mathrm{BB},m} - \mathbf{F}_{\mathrm{R}} \mathbf{Q}_{\mathrm{T},m} \right\|_F^2 \\ \text{s. t.} \; & |\mathbf{F}_{\mathrm{RF}}(i,j)| = \frac{1}{\sqrt{N_T}}, \quad \|\mathbf{F}_{\mathrm{RF}} \mathbf{F}_{\mathrm{BB},m}\|_F^2 = N_s. \end{aligned} \tag{39}$$

Algorithm 2: BAT-MIN algorithm for joint beamforming

Input: $\mathbf{F}_{\mathrm{R}}$, $\mathbf{F}_{\mathrm{C},m}$, δ, tolerable accuracy for BAT-MIN $\epsilon_2 > 0$, maximum iteration for BAT-MIN κ_2, tolerable accuracy for M-BL $\epsilon_3 > 0$ and maximum number of iterations for M-BL κ_3,

Initialization:

- $\mathbf{F}_{\mathrm{RF}}^{(0)}, \mathbf{F}_{\mathrm{BB},m}^{(0)}, \mathbf{Q}_{\mathrm{T},m}^{(0)}$ initialized randomly and the optimization objective in (36) is denoted as $f^{(0)}$, hyperparameters $\widehat{\gamma}_g^{(0)} = 1, \ \forall \ 1 \leqslant g \leqslant G_\theta$, i.e., $\widehat{\mathbf{\Gamma}}^{(0)} = \mathbf{I}_{G_\theta}$, BAT-MIN counter variable $k = 0$, M-BL counter variable $j = 0$ and $\widehat{\mathbf{\Gamma}}^{(-1)} = \mathbf{0}_{G_\theta}$.

while $\left|f^{(k)} - f^{(k-1)}\right| > \epsilon_2$ and $k < \kappa_2$ **do**

$k \leftarrow k + 1$,

Solve sub-problem (37) to compute $\mathbf{Q}_{\mathrm{T},m}$

while $\left\|\widehat{\mathbf{\Gamma}}^{(j)} - \widehat{\mathbf{\Gamma}}^{(j-1)}\right\|_F^2 > \epsilon_3$ and $j < \kappa_3$ **do**

$j \leftarrow j + 1$,

E-Step:

$$\mathbf{\Sigma}^{(j)} = \left(\frac{1}{\sigma_w^2}\mathbf{A}_{\mathrm{T}}^H\mathbf{A}_{\mathrm{T}} + \left(\breve{\mathbf{\Gamma}}^{(j-1)}\right)^{-1}\right)^{-1}$$

$$\boldsymbol{\mathcal{M}}^{(j)} = \frac{1}{\sigma_w^2}\mathbf{\Sigma}^{(j)}\mathbf{A}_{\mathrm{T}}^H\mathbf{\Xi}$$

M-Step: Update the hyperparameters

$$\widehat{\gamma}_g^{(j)} = \frac{1}{N_s}\left\|\boldsymbol{\mathcal{M}}^{(j)}(g,:)\right\|_2^2 + \mathbf{\Sigma}^{(j)}(g,g).$$

end while

M-BL Output: $\breve{\mathbf{F}}_{\mathrm{BB},m}^{(k)} = \boldsymbol{\mathcal{M}}$

Obtain $\mathbf{F}_{\mathrm{BB},m}^{(k)}$ and $\mathbf{F}_{\mathrm{RF}}^{(k)}$ using (48) and procedure discussed thereafter

end while

Output: Optimal $\mathbf{Q}_{\mathrm{T},m}, \mathbf{F}_{\mathrm{BB},m}$ and $\mathbf{F}_{\mathrm{RF}}$

The following matrices can be used for simplifying this problem:

$$\mathbf{P}_1 = \left[\sqrt{\delta}\mathbf{I}_{N_T}, \sqrt{1-\delta}\mathbf{I}_{N_T}\right]^T,$$

$$\mathbf{P}_2 = \left[\sqrt{\delta}\mathbf{F}_{\mathrm{C},m}^T, \sqrt{1-\delta}\mathbf{Q}_{\mathrm{T},m}\mathbf{F}_{\mathrm{R}}^T\right]^T,$$

$$\mathbf{\Xi} = \mathbf{P}_1^H\mathbf{P}_2.$$

The problem (39) can be succinctly derived in a compact form as

$$\begin{aligned}\min_{\mathbf{F}_{\mathrm{RF}},\mathbf{F}_{\mathrm{BB},m}} \ & \|\mathbf{\Xi} - \mathbf{F}_{\mathrm{RF}}\mathbf{F}_{\mathrm{BB},m}\|_F^2 \\ \text{s. t. } & |\mathbf{F}_{\mathrm{RF}}(i,j)| = \frac{1}{\sqrt{N_T}}, \quad \|\mathbf{F}_{\mathrm{RF}}\mathbf{F}_{\mathrm{BB},m}\|_F^2 = P_T.\end{aligned} \tag{40}$$

Furthermore, in order to simultaneously determine the optimal $\mathbf{F}_{\mathrm{BB},m}$ and $\mathbf{F}_{\mathrm{RF}}$, a sparse matrix reconstruction problem is formulated next. As demonstrated in [40], it has been established that the columns of $\mathbf{F}_{\mathrm{RF}}$ can be selected from the set of transmit array steering vectors. Consider $\mathbf{A}_{\mathrm{T}}$ as the quantized transmit array response dictionary matrix that can be expressed as $\mathbf{A}_{\mathrm{T}} = [\mathbf{a}_T(\theta_1), \mathbf{a}_T(\theta_2), \ldots, \mathbf{a}_T(\theta_{G_\theta}))] \in \mathbb{C}^{N_T \times G_\theta}$. The objective of the TPC design problem is to achieve the best approximation to the matrix $\mathbf{\Xi}$, which can be formulated as follows:

$$\begin{aligned}\breve{\mathbf{F}}_{\mathrm{BB},m}^{\mathrm{opt}} &= \arg\min_{\breve{\mathbf{F}}_{\mathrm{BB},m}} \left\|\mathbf{\Xi} - \mathbf{A}_{\mathrm{T}}\breve{\mathbf{F}}_{\mathrm{BB},m}\right\|_F^2, \\ \text{s.t.} &\left\|\mathrm{diag}\left(\breve{\mathbf{F}}_{\mathrm{BB},m}\breve{\mathbf{F}}_{\mathrm{BB},m}^H\right)\right\|_0 \leqslant N_{RF}, \left\|\mathbf{A}_{\mathrm{T}}\breve{\mathbf{F}}_{\mathrm{BB},m}\right\|_F^2 = N_s.\end{aligned} \tag{41}$$

The first constraint arises due to the fact that $\breve{\mathbf{F}}_{\mathrm{BB},m}^{\mathrm{opt}} \in \mathbb{C}^{G_\theta \times N_s}$ can only have N_{RF} non-zero rows associated with the number of active RFCs. This imposes a simultaneous sparse structure on $\breve{\mathbf{F}}_{\mathrm{BB},m}$. The second constraint represents the transmit power constraint as described in (36). Moreover, to leverage the simultaneous sparsity inherent in $\breve{\mathbf{F}}_{\mathrm{BB},m}$, a multiple-measurement vector (MMV) based Bayesian learning (M-BL) regime can be employed. The key motivation for the use of SBL in optimizing ISAC beamforming lies in its robust performance toward achieving sparse solutions. The objective function of SBL, which is derived from a log-likelihood formulation, has fewer local maxima, making it more reliable in evaluating the underlying sparse solution. Additionally, the algorithm leverages the EM method, which is renowned for its ability to ensure convergence. With each iteration, the EM algorithm steadily achieves a lower cost function until it converges to a stable fixed point [21]. This iterative refinement enhances the reliability and effectiveness of the SBL approach. The M-BL technique assigns the following parameterized prior to the matrix $\breve{\mathbf{F}}_{\mathrm{BB},m}$:

$$p\left(\breve{\mathbf{F}}_{\mathrm{BB},m}; \mathbf{\Gamma}\right) = \prod_{g=1}^{G_\theta} p\left(\breve{\mathbf{F}}_{\mathrm{BB},m}(g,:); \gamma_g\right), \tag{42}$$

where γ_g represents the hyperparameter associated with the gth row of $\breve{\mathbf{F}}_{\mathrm{BB},m}$ and the hyperparameter matrix $\mathbf{\Gamma} = \mathrm{diag}(\gamma_1, \gamma_2, \cdots, \gamma_{G_\theta}) \in \mathbb{R}^{G_\theta \times G_\theta}$. The parameterized prior assigned to the N_s-dimensional row vector $\breve{\mathbf{F}}_{\mathrm{BB},m}(g,:)$ is given as $p\left(\breve{\mathbf{F}}_{\mathrm{BB},m}(g,:); \gamma_g\right) \sim \mathcal{CN}(\mathbf{0}, \gamma_g\mathbf{I}_{N_s})$. The key motivation for this prior assignment is that the estimate of $\breve{\mathbf{F}}_{\mathrm{BB},m}(g,:) \to \mathbf{0}$ as the corresponding hyperparameters $\gamma_g \to 0$ [21]. This pertains to the RF TPC column, specified by the beam steering vector for the gth element of the angular grid $\mathcal{G}(\theta)$. The a posterior density of $\breve{\mathbf{F}}_{\mathrm{BB},m}$ can be computed as $p\left(\breve{\mathbf{F}}_{\mathrm{BB},m}(:,s) \mid \mathbf{\Xi}(:,s); \mathbf{\Gamma}\right) \sim \mathcal{CN}(\boldsymbol{\mathcal{M}}(:,s), \mathbf{\Sigma})$, for all $1 \leqslant s \leqslant N_s$, where the posterior mean $\boldsymbol{\mathcal{M}}$ and covariance $\mathbf{\Sigma}$ are expressed as

$$\boldsymbol{\mathcal{M}} = \frac{1}{\sigma_w^2}\mathbf{\Sigma}\mathbf{A}_{\mathrm{T}}^H\mathbf{\Xi}, \quad \mathbf{\Sigma} = \left(\frac{1}{\sigma_w^2}\mathbf{A}_{\mathrm{T}}^H\mathbf{A}_{\mathrm{T}} + (\mathbf{\Gamma})^{-1}\right)^{-1}, \tag{43}$$

and σ_w^2 represents the variance of the approximation error. It is evident from (43) that the determination of $\breve{\mathbf{F}}_{\mathrm{BB},m}$ relies on the hyperparameter matrix $\mathbf{\Gamma}$. Therefore, the estimation problem of $\breve{\mathbf{F}}_{\mathrm{BB},m}$ simplifies to the estimation of the corresponding hyperparameter vector $\boldsymbol{\gamma} = [\gamma_1, \gamma_2, \cdots, \gamma_{G_\theta}]^T$. The iterative EM algorithm can now be employed for maximizing the Bayesian evidence $p(\mathbf{\Xi}; \mathbf{\Gamma})$. Toward this, in the E-step of the

TABLE II: Parameters used for ISAC System-1 and System-2

Parameters	**System-1**	**System-2**	**Parameters**	**System-1**	**System-2**
System bandwidth, B	1.92 MHz	5.12 MHz	# DFRC BS RFCs, N_{RF}	8	8
Subcarrier Spacing, Δf	120 kHz	160 kHz	# UE antenna, M_R	8	10
# subcarriers, M	16	32	DFRC Velocity resolution (m/s), $\Delta V = c/2f_cN_pT_s$	73.05	47.62
# OFDM pilot Symbols in a frame, N_p	8	16	Range resolution (m), $\Delta R = c/2B$	78.12	29.30
Cyclic prefix duration, T_{cp}	$0.1T$	$0.125T$	DFRC angular resolution, $\Delta\theta^\circ$	10°	5°
# Scatterers, L	2	3	Doppler bins, G_ν	8	12
# Targets, P	3	6	Delay bins, G_τ	8	12
# DFRC TAs/RAs, N_T/ N_R	16	32	Angular bins, G_θ/G_ϑ	18	36

TABLE III: Computational complexity for (a) 3D-BL (b) BAT-MIN and (c) MUSIC

(a) 3D-BL

Operation	**Complexity order**
$\boldsymbol{\Sigma}_r^{(j)}$	$\mathcal{O}(G_\tau^3G_\nu^3G_\theta^3)$
$\boldsymbol{\alpha}^{(j)}$	$\mathcal{O}(G_\tau^2G_\nu^2G_\theta^2)$
$\omega_r^{(j)}$	$\mathcal{O}(G_\tau G_\nu G_\theta)$

(b) BAT-MIN

Operation	**Complexity order**
$\boldsymbol{\Sigma}^{(j)}$	$\mathcal{O}(G_\theta^3)$
$\mathcal{M}^{(j)}$	$\mathcal{O}(N_sG_\theta^2)$
$\gamma_g^{(j)}$	$\mathcal{O}(N_sG_\theta)$

(c) MUSIC, G_m: number of spectral grids

Operation	**Complexity order**
Covariance $\mathbf{R}_y$ calculation	$\mathcal{O}(M_R^2MN_p)$
Eigenvalue decomposition	$\mathcal{O}(M_R^3)$
Noise subspace construction	$\mathcal{O}((M_R-L)M_R^2)$
Spectral search	$\mathcal{O}(M_R^2G_m)$

jth iteration, the average log-likelihood $\mathcal{L}\left(\boldsymbol{\Gamma} \mid \widehat{\boldsymbol{\Gamma}}^{(j-1)}\right)$ for the complete dataset is computed which is expressed as:

$$\mathcal{L}\left(\boldsymbol{\Gamma} \mid \widehat{\boldsymbol{\Gamma}}^{(j-1)}\right) = \mathbb{E}_{\breve{\mathbf{F}}_{\mathrm{BB},m}|\boldsymbol{\Xi};\widehat{\boldsymbol{\Gamma}}^{(j-1)}}\left\{\log p\left(\boldsymbol{\Xi}, \breve{\mathbf{F}}_{\mathrm{BB},m}; \boldsymbol{\Gamma}\right)\right\}. \tag{44}$$

Subsequently, in the M-step, the maximization is performed for $\mathcal{L}\left(\boldsymbol{\Gamma} \mid \widehat{\boldsymbol{\Gamma}}^{(j-1)}\right)$ with respect to the hyperparameter vector γ, yielding the estimate

$$\begin{aligned}\widehat{\gamma}^{(j)} = \arg\max_{\boldsymbol{\gamma}} \mathbb{E}_{\breve{\mathbf{F}}_{\mathrm{BB},m}|\boldsymbol{\Xi};\widehat{\boldsymbol{\Gamma}}^{(j-1)}}\Big\{&\log p\left(\boldsymbol{\Xi} \mid \breve{\mathbf{F}}_{\mathrm{BB},m}\right) \\ &+ \log p\left(\breve{\mathbf{F}}_{\mathrm{BB},m}; \boldsymbol{\Gamma}\right)\Big\}.\end{aligned} \tag{45}$$

The first term in (45) is observed to be independent of the hyperparameter vector γ and can, therefore, be discarded during the maximization in the M-step. The corresponding optimization problem of estimating the hyperparameter vector γ can be simplified as

$$\begin{aligned}\widehat{\boldsymbol{\gamma}}^{(j)} &= \arg\max_{\boldsymbol{\gamma}} \mathbb{E}_{\breve{\mathbf{F}}_{\mathrm{BB},m}|\boldsymbol{\Xi};\widehat{\boldsymbol{\Gamma}}^{(j-1)}}\left\{\log p\left(\breve{\mathbf{F}}_{\mathrm{BB},m}; \boldsymbol{\Gamma}\right)\right\} \\ &= \arg\max_{\gamma} \sum_{g=1}^{G_\theta} -N_s\log\left(\pi\gamma_g\right) - \frac{\left\|\boldsymbol{\mathcal{M}}^{(j)}(g,:)\right\|^2 + N_s\boldsymbol{\Sigma}^{(j)}(g,g)}{\gamma_g},\end{aligned} \tag{46}$$

where $\boldsymbol{\mathcal{M}}^{(j)}$ and $\boldsymbol{\Sigma}^{(j)}$ are obtained from (43) by setting $\boldsymbol{\Gamma} = \widehat{\boldsymbol{\Gamma}}^{(j-1)}$. By setting the gradient of the objective function in (45) with respect to $\boldsymbol{\gamma}$ to zero, we can determine the estimate of γ_g during the jth iteration of the EM algorithm as

$$\widehat{\gamma}_g^{(j)} = \frac{1}{N_s}\left\|\boldsymbol{\mathcal{M}}^{(j)}(g,:)\right\|_2^2 + \boldsymbol{\Sigma}^{(j)}(g,g). \tag{47}$$

Upon convergence, we aim at $\breve{\mathbf{F}}_{\mathrm{BB},m} = \boldsymbol{\mathcal{M}}^{(j)}$. The baseband TPC matrix $\mathbf{F}_{\mathrm{BB},m}$ can be derived from $\breve{\mathbf{F}}_{\mathrm{BB},m}$ by first obtaining the largest N_{RF} hyperparameters and their indices. Let $\mathcal{I}$ denote the set of the row indices corresponding to the largest hyperparameters. Then the unnormalized baseband TPC matrix $\mathbf{F}_{\mathrm{BB},m}$ can be expressed as

$$\mathbf{F}_{\mathrm{BB},m} = \breve{\mathbf{F}}_{\mathrm{BB},m}(\mathcal{I},:). \tag{48}$$

Subsequently, the RF TPC denoted as $\mathbf{F}_{\mathrm{RF}}$ can be derived from $\mathbf{A}_{\mathrm{T}}$ by selecting the N_{RF} columns that align with the rows extracted from $\breve{\mathbf{F}}_{\mathrm{BB},m}$. Finally, the baseband TPC is then normalized as $\mathbf{F}_{\mathrm{BB},m} \leftarrow \frac{\sqrt{N_s}}{\|\mathbf{F}_{\mathrm{RF}}\mathbf{F}_{\mathrm{BB},m}\|_F}\mathbf{F}_{\mathrm{BB},m}$ to satisfy the power constraint. Algorithm-2 provides a concise overview of this procedure.

It is important to mention that the proposed BAT-MIN algorithm can also be adapted for dynamic RFC selection in scenarios, where the number of targets and scatterers is not known a priori [34]. The number of dominant hyperparameters obtained at the convergence of the algorithm can be utilized to activate the minimum number of RF chains necessary for closely approximating the ideal digital precoder or combiner, hence offering better energy efficiency.

VI. Computational complexity

The computational complexity of the proposed 3D-BL technique is of the order $\mathcal{O}(G_\tau^3G_\nu^3G_\theta^3)$ per iteration due to the inversion of the matrix $\boldsymbol{\Sigma}_r \in \mathbb{C}^{G_\tau G_\nu G_\theta \times G_\tau G_\nu G_\theta}$. Similarly, the complexity of the BAT-MIN algorithm is of the order $\mathcal{O}(G_\theta^3)$ per iteration due to the inversion of $\boldsymbol{\Sigma} \in \mathbb{C}^{G_\theta \times G_\theta}$. The MUSIC algorithm requires $\mathcal{O}(M_R^3)$ operations due to the eigenvalue decomposition of the covariance matrix $\mathbf{R}_y \in \mathbb{C}^{M_R \times M_R}$. A detailed description of computational complexity is given in Table. III.

VII. Simulation Results

This section characterizes the performance of the 3D-BL and BAT-MIN techniques proposed for radar target parameter estimation and DFRC beamformer designs, respectively. System-1 and System-2, have been examined, and the various simulation parameters used are provided in Table II. The targets are dispersed randomly in the scattering environment, and the RCS coefficients of these targets are generated as random variables, following a distribution denoted as $\alpha_p \sim \mathcal{CN}(0,1)$. A similar distribution is followed by β_ℓ. For the estimation based on BL, the stopping parameters are configured as $\epsilon_1 = \epsilon_2 = \epsilon_3 = 10^{-6}$ and $\kappa_1 = \kappa_2 = \kappa_3 = 50$. The

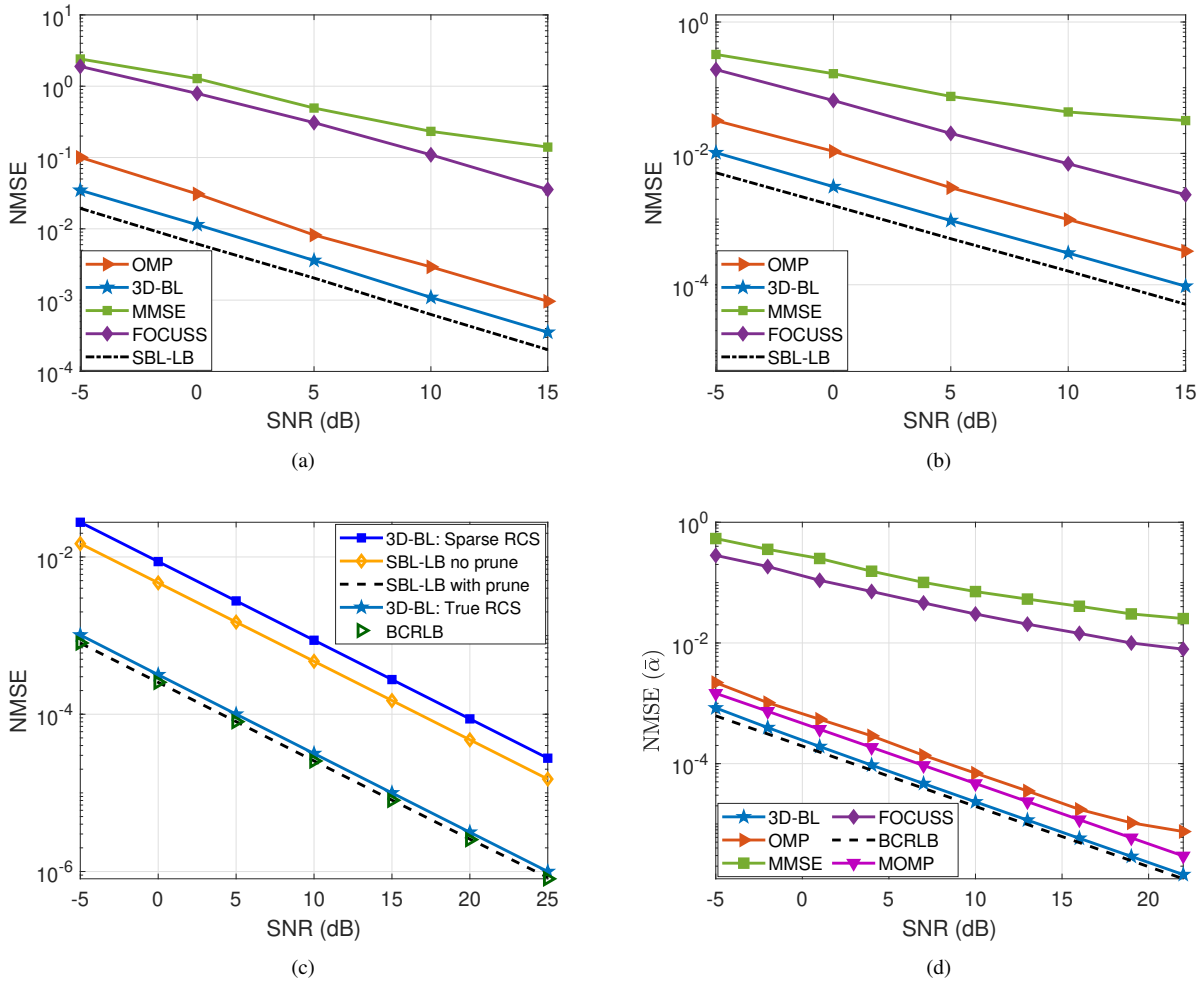

Fig. 2: (a) NMSE versus SNR performance of sparse RCS estimation for System-1; (b) System-2; (c) BCRLB and SBL-LB comparison; (d) NMSE versus SNR performance of true RCS estimation for System-1.

regularization parameter for FOCUSS is set to $0.1\sigma^2$, the l_p-norm parameter is adjusted to $p = 0.8$ with a stopping threshold of $\epsilon = 10^{-6}$, and the maximum number of iterations is set to $N_{\max} = 800$.

A. *Radar parameter estimation*

Fig. 2a and 2b depict a comparison of the NMSE performance for the proposed 3D-BL schemes designed for the 3D-sparse radar model, in contrast to the OMP, FOCUSS, and MMSE techniques. The outcomes are illustrated separately for System-1 and System-2 in Fig. 2a and Fig. 2b, respectively. Furthermore, the efficiency of the proposed techniques is assessed by comparing them against the SBL-LB derived in (56). The NMSE of the RCS estimate for the radar target is defined as NMSE $\triangleq \frac{\|\hat{\boldsymbol{\alpha}}-\boldsymbol{\alpha}\|_2^2}{\|\boldsymbol{\alpha}\|_2^2}$.

In Fig. 2a, a notable NMSE gain of approximately 5 dB and 15 dB is observed for the proposed 3D-BL techniques when compared to OMP and FOCUSS, respectively. The OMP algorithm suffers due to its dependence on both the choice of the sensing matrix and on the threshold, hence requiring careful empirical tuning. Even a slight variation in the stopping parameters may result in convergence and structural errors. Furthermore, each incorrect column selection in an iteration has a cascading effect, leading to error propagation [21]. FOCUSS also faces limitations due to convergence issues and its susceptibility to the regularization parameter [41]. The NMSE performance of the MMSE estimator is notably suboptimal, which is attributed to its failure to leverage the inherent sparsity in the parameter $\boldsymbol{\alpha}$. This observation underscores the significance of incorporating sparsity-aware techniques for enhancing the estimation accuracy in our study. A significant NMSE performance improvement of 10 dB is observed for 3D-BL in System-2 over System-1. This is attributed to the difference in the number of observations, which is $N_{RF}MN_p = 4096$ for System-2, whereas it is 1024 for System-1. This increase in observations provides better estimation accuracy [42].

Fig. 2c shows the comparison of SBL-LB and BCRLB derived in the appendix. The SBL-LB serves as a lower bound for the sparse RCS vector $\boldsymbol{\alpha} \in \mathbb{C}^{G_\tau G_\nu G_\theta \times 1}$, while the BCRLB operates under the assumption of perfect knowledge of all parameters except the true RCS coefficient provides the lower bound for the true RCS coefficients $\bar{\boldsymbol{\alpha}} \in \mathbb{C}^{P\times 1}$. The SBL-LB requires the hyperparameter matrix $\boldsymbol{\Omega}$, which is esti-

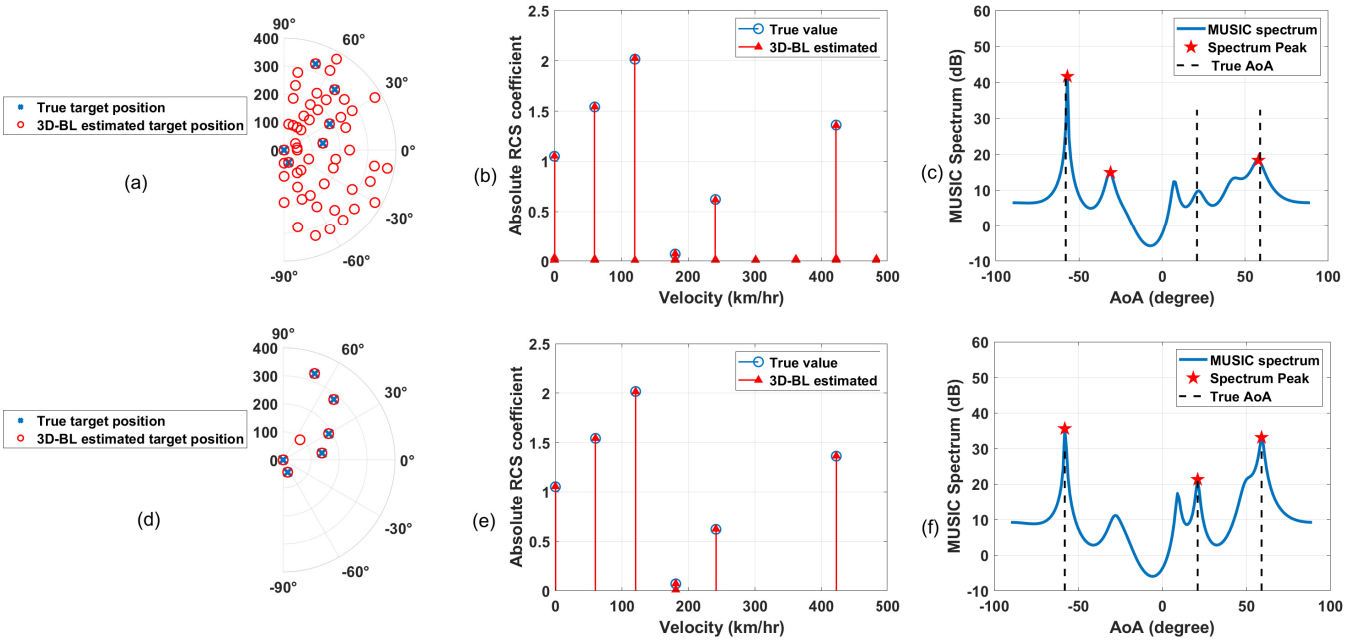

Fig. 3: Demonstration of the parameter estimation of System-II at SNR= -5 dB and SNR= 5 dB. (a) Estimated AoA and range by 3D-BL at SNR $= -5$ dB (b) Estimated absolute RCS coefficients versus velocity estimated by 3D-BL at SNR $= -5$ dB (c) MUSIC spectrum of AoA at the UE at SNR $= -5$ dB (d) Estimated AoA and range estimated at SNR $= 5$ dB (e) Estimated absolute RCS coefficients versus velocities estimated by 3D-BL at SNR $= 5$ dB (f) MUSIC spectrum of AoA at the UE at SNR $= 5$ dB.

mated during the 3D-BL process. While these hyperparameters should ideally be zero at non-support locations, some small values still appear in estimation. By pruning these small values and replacing them with near-zero values, the hyperparameter matrix $\mathbf{\Omega}$ approaches its ideal value, bringing the SBL-LB closer to the BCRLB, as shown in Fig. 2c. Fig. 2d shows the NMSE of true RCS for 3D-BL, also compared against the multi-dimensional OMP (MOMP) [43]. While MOMP uses smaller, decoupled dictionaries for each parameter dimension, 3D-BL employs a global dictionary that jointly captures delay, Doppler, and angle information. This joint modeling increases computational complexity but enables superior recovery. As shown in Fig. 2d, while MOMP performs slightly better than the OMP, 3D-BL outperforms MOMP by about 3 dB, justifying its higher complexity.

B. Imaging

Once the estimate of the RCS vector $\widehat{\boldsymbol{\alpha}}$ has been obtained using the 3D-BL, imaging of the scattering scene can be conducted. The reliable detection of any target in the delay, Doppler, and angle bin (i, j, k) is confirmed if $|\widehat{\alpha}(i, j, k)| > \eta$, where $\eta \ll 1$ is a carefully chosen threshold. Moreover, let $\mathcal{T}$ represent the set of all bins (i, j, k) satisfying the detection criterion, which can be expressed as $\mathcal{T} = \{(i, j, k) \mid |\widehat{\alpha}(i, j, k)| > \eta\}$. Then the number of targets that can be detected is given by $\widehat{P} = |\mathcal{T}|$. The range, velocity and AoA of the pth target can be estimated by

$$\widehat{R}_p = \frac{c}{2M\Delta f}\widehat{i}, \quad \widehat{v}_p = \frac{c}{2f_c N_p T_s}\widehat{j} \quad \widehat{\theta}_p = \frac{\pi}{G_\theta}\widehat{k}. \tag{49}$$

Furthermore, the Cartesian coordinates $(\hat{x}_p, \hat{y}_p)$ of the pth target, relative to the BS located at the origin, can be determined from the estimated AoA $\hat{\theta}_p$ and range $\hat{R}_p$ as follows:

$$\hat{x}_p = \hat{R}_p \cos\hat{\theta}_p, \quad \hat{y}_p = \hat{R}_p \sin\hat{\theta}_p.$$

Fig. 3(a)-(c) and 3(e)-(g) illustrate the imaging performance of the proposed 3D-BL scheme at SNR $= -5$ dB and SNR $= 5$ dB, respectively, where the detection threshold is set to $\eta = 0.01$. In 3(a) and 3(b), the polar scatter plots representing the angle-range information of the targets are displayed for SNR $= -5$ dB and SNR $= 5$ dB, respectively. Even at SNR $= -5$ dB, the positions of all six targets are accurately estimated, albeit with a relatively high false positive rate. This false positive rate is notably reduced at SNR $= 5$ dB, and the angle-range information of the targets is estimated with high precision. Fig. 3(c) and 3(d) depict the efficacy of the proposed 3D-BL in terms of both velocity and RCS parameter estimation. At low SNRs, such as SNR $= -5$ dB, some false positives can also be seen. However, it is interesting to see from Fig. 3 (c) that while false positives exist at low SNR, their magnitude is weak. This type-I error rate is significantly reduced at SNR $= 5$ dB. In addition, Figures 3(e) and 3(f) showcase the efficiency of AoA estimation at the UE using MUSIC. The MUSIC spectrum in 3(e) reveals that at such low SNRs, the estimation of the angle of two communication scatterers is very close to the true AoA, while an erroneous estimation occurs at an angle of -30° corresponding to the true location at 20°. However, at SNR $= 5$ dB, all the angles of the communication scatterers are accurately estimated.

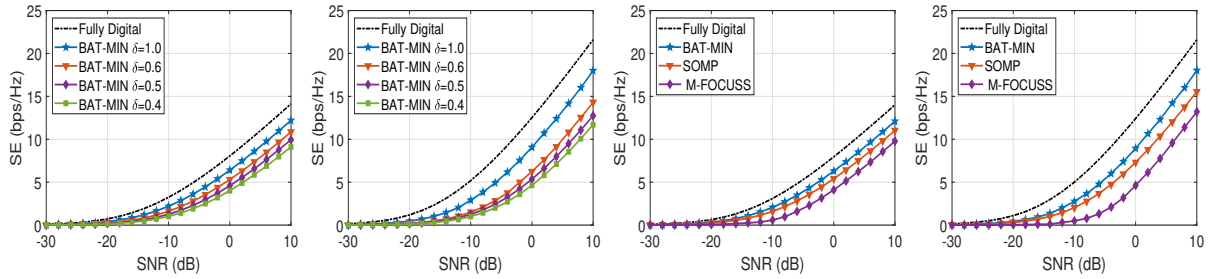

Fig. 4: Spectral efficiency achieved by the fully digital precoder and BAT-MIN algorithm with different values of δ for (a) System-1; (b) System-2. Spectral efficiency achieved by different hybrid beamforming algorithms at $\delta = 1$ for (c) System-1; (d) System-2.

C. Spectral efficiency

Fig. 4a and 4b shows the spectral efficiency achieved by the proposed BAT-MIN algorithm for the weighting factor values $\delta = \{0.4, 0.5, 0.6, 1\}$, corresponding to System-1 and System-2, respectively. The performance of the proposed scheme is also contrasted to that of the optimal FD beamformer in these plots. It is evident that as δ increases, the SE also increases, indicating a higher weight allocated to obtaining the hybrid communication beamformer, which approaches the performance of the optimal FD beamformer. Moreover, a capacity difference of 3 bps/Hz can be observed between $\delta = 0.4$ and $\delta = 1$ at SNR=10 dB. This divergence arises due to the allocation of higher weight to the radar beamformer when $\delta = 0.4$, thereby eroding the communication performance. Even at $\delta = 0.4$, when the beamformer is more biased towards the radar side, a SE of 10 bps/Hz can be obtained. Furthermore, the SE difference between the proposed BAT-MIN algorithm at $\delta = 1$ and the optimal FD beamformer is marginal at 2 bps/Hz. It is also interesting to see that the proposed algorithm achieves a performance close to the optimal FD beamformer, especially in the low-SNR region, regardless of the value of δ.

Fig. 4c and 4d compare the SE performance of the BAT-MIN algorithm to other competing schemes. Here the SOMP and M-FOCUSS are the alternating minimization algorithms associated with SOMP and M-FOCUSS used for the design of $\breve{\mathbf{F}}_{\mathrm{BB},m}$. It is evident that the proposed BAT-MIN algorithm results in a 1 bps/Hz SE improvement over the SOMP-based alternating minimization. Moreover, the M-FOCUSS-based alternating minimization algorithm exhibits a 2 bps/Hz SE loss over the proposed BAT-MIN algorithm. These observations are in line with our previous discussion of the NMSE performance seen for the OMP and FOCUSS. Within the class of sparse beamforming algorithms, SOMP stands as a potential competitor [14]. However, SOMP, being a greedy algorithm, exhibits sensitivity both to the selection of the dictionary matrix and to the stopping criterion, which impacts its performance. By contrast, as demonstrated in our simulations, the proposed SBL approach consistently outperforms SOMP and other state-of-the-art methods in ISAC beamforming, highlighting its effectiveness and reliability.

One can also observe the SE improvement of System-2 as compared to System-1. This improvement is attributed to an increase in the number of communication paths in System-2, which is $L = 3$, in contrast to $L = 2$ for System-1. This improves the rank of the communication channel, resulting in the observed SE improvement of System-2.

D. Beampattern

Fig. 6 shows the beampatterns of the proposed BAT-MIN beamformer along with $\delta = \{0.1, 0.5, 0.9\}$, $P = 5$ and $L = 2$. The proposed beampattern is also compared to the ideal radar and communication beampattern. It can be observed that at $\delta = 0.1$ the radar operation dominates, and hence the DFRC beamformer can effectively steer beams in the direction of the targets along negligible directivity towards the communication scatterers. On the other hand, a trade-off between sensing and communication is noticeable at $\delta = 0.5$, where the proposed DFRC beamformer succeeds in forming beams towards all the targets and scatterers. One observes that at $\delta = 0.9$, namely when the communication operation dominates, the DFRC beamformer effectively steers the beams toward the communication scatterers, with no beams toward the targets. It is also interesting to note that in all the cases, the side lobes are weaker than the side lobes of the ideal communication beamformer, which shows the effectiveness of the proposed beamformer.

VIII. Summary and Conclusion

We introduced a representation of the radar channel in the delay-Doppler-angular domain and subsequently derived the end-to-end relationship of a mmWave MIMO-OFDM ISAC system. Subsequently, an innovative radar parameter estimation model was developed, exploiting the inherent three-dimensional sparse structure of the radar channel, followed by the development of a radar parameter estimation model to exploit the inherent 3D-sparsity. The proposed 3D-BL framework achieved superior NMSE performance compared to its competitors, like the OMP, FOCUSS, and MMSE-based schemes. Furthermore, a zero-forcing beamformer was utilized to reduce the system complexity to estimate the uplink parameters. Moreover, we introduced an innovative technique that leverages Bayesian learning in conjunction with an alternating minimization algorithm for joint beamformer design. This addition represents a significant advancement in optimizing

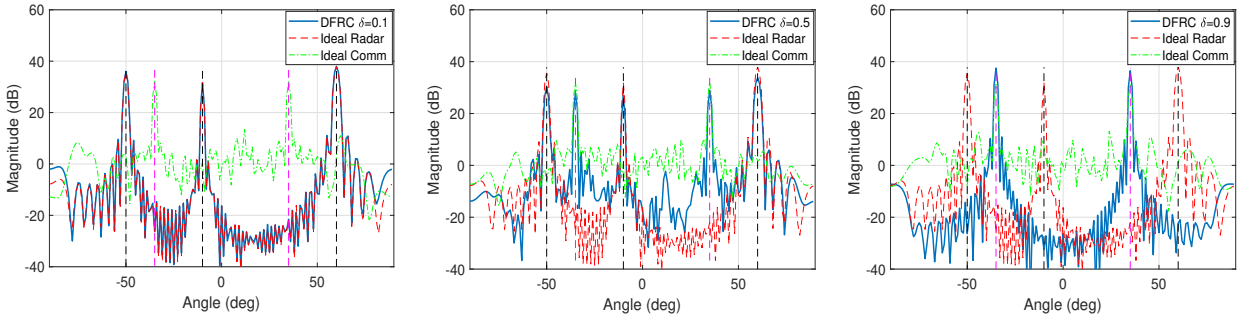

(a) (b) (c)

Fig. 5: BAT-MIN DFRC beampattern of System-1 for (a) $\delta = 0.1$; (b) $\delta = 0.5$; (c) $\delta = 0.9$.

the beamforming process within a mmWave MIMO-OFDM ISAC system, which ultimately enhanced the system's overall performance and related capabilities.

The simulation results undeniably validate the effectiveness of the proposed 3D-BL schemes, showcasing its commendable performance that closely aligns with the SBL-LB. Noteworthy is the substantial improvement of at least 5 dB compared to alternative techniques. Furthermore, the proposed BAT-MIN beamformer stands out as a formidable solution, closely rivaling the capabilities of a fully digital beamformer and maintaining a significant minimum advantage of 1 bps/Hz over its peers. These collective findings emphasize the substantial significance and practical efficacy of the proposed techniques.

IX. Appendix

A. Bayesian Cramér-Rao lower bound

Let us define the radar channel $\mathbf{H}_{n,m}^r$ in the compact form as $\mathbf{H}_{n,m}^r = \mathbf{A}_R\mathbf{R}_m\mathbf{C}\mathbf{D}_n\mathbf{A}_T^H$, where $\mathbf{A}_R = [\mathbf{a}_R(\theta_1),\ldots,\mathbf{a}_R(\theta_P)] \in \mathbb{C}^{N_R\times L}$ and $\mathbf{A}_T = [\mathbf{a}_T(\theta_1),\ldots,\mathbf{a}_T(\theta_P)] \in \mathbb{C}^{N_T\times L}$. The matrices $\mathbf{R}_m, \mathbf{C}, \mathbf{D}_n \in \mathbb{C}^{P\times P}$ are diagonal matrices whose pth diagonal entries are $e^{-\mathrm{j}2\pi m\Delta f\tau_p}$, α_p and $e^{\mathrm{j}2\pi nT_s\nu_p}$, respectively. Note that for BCRLB derivation we assume that the parameters θ_p, τ_p, ν_p are assumed to be known for $1 \leqslant p \leqslant P$, and the RCS coefficients α_p are to be estimated. Based on the system model of (1), we have:

$$\begin{aligned}\mathbf{y}_{\text{echo}}(n,m) &= \mathbf{W}_{\text{RF}}^H\mathbf{A}_R\mathbf{R}_m\mathbf{C}\mathbf{D}_n\mathbf{A}_T^H\mathbf{F}_{\text{RF}}\mathbf{x}_{n,m} + \mathbf{W}_{\text{RF}}^H\mathbf{v}_{n,m},\\ &= \mathbf{\Psi}_{n,m}\bar{\boldsymbol{\alpha}} + \tilde{\mathbf{v}}_{n,m},\end{aligned}$$

where $\mathbf{\Psi}_{n,m} = (\mathbf{x}_{n,m}^T\mathbf{F}_{\text{RF}}\mathbf{A}_T^*\mathbf{D}_n^T \odot \mathbf{W}_{\text{RF}}^H\mathbf{A}_R\mathbf{R}_m) \in \mathbb{C}^{N_{RF}\times L}$ and $\bar{\boldsymbol{\alpha}} = [\alpha_1,\ldots,\alpha_P]^T \in \mathbb{C}^{L\times 1}$. Following the procedure from (11) to (12), the stacked observations corresponding to M subcarriers and N_p training OFDM symbols can be obtained as

$$\mathbf{y}_r = \mathbf{\Psi}_r\bar{\boldsymbol{\alpha}} + \mathbf{v}_r. \tag{50}$$

Since this is a linear model, both the best linear unbiased estimator (BLUE) and the Cramer-Rao bound (CRB) $\bar{\boldsymbol{\alpha}}$ can be derived as $\hat{\bar{\boldsymbol{\alpha}}} = \mathbf{\Psi}_r^\dagger\mathbf{y}_r$, while the BCRLB of $\hat{\bar{\boldsymbol{\alpha}}}$ associated with $\mathbf{R}_\alpha = \mathbf{I}$ is formulated as [44]

$$\mathbb{E}\left[(\hat{\bar{\boldsymbol{\alpha}}} - \bar{\boldsymbol{\alpha}})(\hat{\bar{\boldsymbol{\alpha}}} - \bar{\boldsymbol{\alpha}})^H\right] \geqslant (\mathbf{\Psi}_r^H\mathbf{R}_v^{-1}\mathbf{\Psi}_r + \mathbf{R}_\alpha^{-1})^{-1} \tag{51}$$

$$\implies \text{MSE}(\hat{\bar{\boldsymbol{\alpha}}}) \geqslant \text{Tr}\left\{(\mathbf{\Psi}_r^H\mathbf{R}_v^{-1}\mathbf{\Psi}_r + \mathbf{R}_\alpha^{-1})^{-1}\right\}. \tag{52}$$

B. SBL-lower bound

In this section, the SBL-LB of the proposed 3D-BL scheme is derived. The Bayesian Fisher Information matrix (FIM) $\mathbf{J}_T \in \mathbb{C}^{G_\tau G_\nu G_\theta \times G_\tau G_\nu G_\theta}$ for the linear model of (12) can be determined as $\mathbf{J}_T = \mathbf{J}_y + \mathbf{J}_\alpha$, where $\mathbf{J}_y \in \mathbb{C}^{G_\tau G_\nu G_\theta \times G_\tau G_\nu G_\theta}$ and $\mathbf{J}_\alpha \in \mathbb{C}^{G_\tau G_\nu G_\theta \times G_\tau G_\nu G_\theta}$ are the FIMs associated with the observation vector $\mathbf{y}_r$ and RCS vector $\boldsymbol{\alpha}$, respectively. The matrices $\mathbf{J}_y$ and $\mathbf{J}_\alpha$ can be defined as

$$\mathbf{J}_y = -\mathbb{E}_{(\mathbf{y}_r,\boldsymbol{\alpha})}\left\{\frac{\partial^2\mathcal{L}(\mathbf{y}_r|\boldsymbol{\alpha})}{\partial\boldsymbol{\alpha}\partial\boldsymbol{\alpha}^H}\right\}, \mathbf{J}_\alpha = -\mathbb{E}_{\boldsymbol{\alpha}}\left\{\frac{\partial^2\mathcal{L}(\boldsymbol{\alpha};\mathbf{\Omega})}{\partial\boldsymbol{\alpha}\partial\boldsymbol{\alpha}^H}\right\}, \tag{53}$$

where $\mathcal{L}(\mathbf{y}_r|\boldsymbol{\alpha}) = \log p(\mathbf{y}_r|\boldsymbol{\alpha})$ and $\mathcal{L}(\boldsymbol{\alpha};\mathbf{\Omega}) = \log p(\boldsymbol{\alpha};\mathbf{\Omega})$ are the log-likelihood of the observation and log-prior density of the RCS vector $\boldsymbol{\alpha}$, which can be expressed as

$$\begin{aligned}\mathcal{L}(\mathbf{y}_r|\boldsymbol{\alpha}) &= \varpi_1 - (\mathbf{y}_r - \mathbf{\Phi}_r\boldsymbol{\alpha})^H\mathbf{R}_v^{-1}(\mathbf{y}_r - \mathbf{\Phi}_r\boldsymbol{\alpha}),\\ \mathcal{L}(\boldsymbol{\alpha};\mathbf{\Omega}) &= \varpi_2 - \boldsymbol{\alpha}^H\mathbf{\Omega}^{-1}\boldsymbol{\alpha}.\end{aligned} \tag{54}$$

The constant terms ϖ_1 and ϖ_2 are derived as

$$\begin{aligned}\varpi_1 &= -N_{RF}MN_p\log\pi - \log\det(\mathbf{R}_v),\\ \varpi_2 &= -G_\tau G_\nu G_\theta\log\pi - \log\det(\mathbf{\Omega}).\end{aligned} \tag{55}$$

Now, by substituting (54) and (55) into (53), one can obtain $\mathbf{J}_y = \mathbf{\Phi}_r^H\mathbf{R}_v^{-1}\mathbf{\Phi}_r$ and $\mathbf{J}_\alpha = \mathbf{\Omega}^{-1}$. Therefore, the Bayesian FIM $\mathbf{J}_T$ can be formulated as $\mathbf{J}_T = \mathbf{\Phi}_r^H\mathbf{R}_v^{-1}\mathbf{\Phi}_r + \mathbf{\Omega}^{-1}$. Hence, the SBL-LB for the MSE of the estimation of the RCS vector $\boldsymbol{\alpha}$ can be expressed as

$$\text{MSE}(\hat{\boldsymbol{\alpha}}) \geqslant \text{Tr}\left(\mathbf{J}_T^{-1}\right). \tag{56}$$

References

[1] C.-X. Wang, X. You, X. Gao, X. Zhu, Z. Li, C. Zhang, H. Wang, Y. Huang, Y. Chen, H. Haas *et al.*, "On the road to 6G: Visions, requirements, key technologies and testbeds," *IEEE Communications Surveys & Tutorials*, 2023.

[2] B. Paul, A. R. Chiriyath, and D. W. Bliss, "Survey of RF communications and sensing convergence research," *IEEE Access*, vol. 5, pp. 252–270, 2016.

[3] S. Lu, F. Liu, Y. Li, K. Zhang, H. Huang, J. Zou, X. Li, Y. Dong, F. Dong, J. Zhu, Y. Xiong, W. Yuan, Y. Cui, and L. Hanzo, "Integrated sensing and communications: Recent advances and ten open challenges," *IEEE Internet of Things Journal*, pp. 1–1, 2024.

[4] J. Wang, N. Varshney, C. Gentile, S. Blandino, J. Chuang, and N. Golmie, "Integrated sensing and communication: Enabling techniques, applications, tools and data sets, standardization, and future directions," *IEEE Internet of Things Journal*, vol. 9, no. 23, pp. 23 416–23 440, 2022.

[5] F. Liu, L. Zheng, Y. Cui, C. Masouros, A. P. Petropulu, H. Griffiths, and Y. C. Eldar, "Seventy years of radar and communications: The road from separation to integration," *IEEE Signal Processing Magazine*, vol. 40, no. 5, pp. 106–121, 2023.

[6] P. Kumari, A. Mezghani, and R. W. Heath, "JCR70: A low-complexity millimeter-wave proof-of-concept platform for a fully-digital SIMO joint communication-radar," *IEEE Open Journal of Vehicular Technology*, vol. 2, pp. 218–234, 2021.

[7] H. Wymeersch, G. Seco-Granados, G. Destino, D. Dardari, and F. Tufvesson, "5G mmWave positioning for vehicular networks," *IEEE Wireless Communications*, vol. 24, no. 6, pp. 80–86, 2017.

[8] C. Yang and H.-r. Shao, "WiFi-based indoor positioning," *IEEE Communications Magazine*, vol. 53, no. 3, pp. 150–157, 2015.

[9] S. Zhang, Y. Zeng, and R. Zhang, "Cellular-enabled UAV communication: A connectivity-constrained trajectory optimization perspective," *IEEE Trans. on Communications*, vol. 67, no. 3, pp. 2580–2604, 2019.

[10] K. V. Mishra, M. Bhavani Shankar, V. Koivunen, B. Ottersten, and S. A. Vorobyov, "Toward millimeter-wave joint radar communications: A signal processing perspective," *IEEE Signal Processing Magazine*, vol. 36, no. 5, pp. 100–114, 2019.

[11] T. S. Rappaport, S. Sun, R. Mayzus, H. Zhao, Y. Azar, K. Wang, G. N. Wong, J. K. Schulz, M. Samimi, and F. Gutierrez, "Millimeter wave mobile communications for 5G cellular: It will work!" *IEEE access*, vol. 1, pp. 335–349, 2013.

[12] H. Wymeersch, G. Seco-Granados, G. Destino, D. Dardari, and F. Tufvesson, "5G mmwave positioning for vehicular networks," *IEEE Wireless Communications*, vol. 24, no. 6, pp. 80–86, 2017.

[13] M. R. Akdeniz, Y. Liu, M. K. Samimi, S. Sun, S. Rangan, T. S. Rappaport, and E. Erkip, "Millimeter wave channel modeling and cellular capacity evaluation," *IEEE Journal on Selected Areas in Communications*, vol. 32, no. 6, pp. 1164–1179, 2014.

[14] R. W. Heath, N. Gonzalez-Prelcic, S. Rangan, W. Roh, and A. M. Sayeed, "An overview of signal processing techniques for millimeter wave MIMO systems," *IEEE journal of selected topics in signal processing*, vol. 10, no. 3, pp. 436–453, 2016.

[15] Z. Pi and F. Khan, "An introduction to millimeter-wave mobile broadband systems," *IEEE comm. magazine*, vol. 49, no. 6, pp. 101–107, 2011.

[16] C. Sturm and W. Wiesbeck, "Waveform design and signal processing aspects for fusion of wireless communications and radar sensing," *Proceedings of the IEEE*, vol. 99, no. 7, pp. 1236–1259, 2011.

[17] T. Tian, T. Zhang, L. Kong, and Y. Deng, "Transmit/receive beamforming for MIMO-OFDM based dual-function radar and communication," *IEEE Trans. on Vehicular Tech.*, vol. 70, no. 5, pp. 4693–4708, 2021.

[18] C. Shi, Y. Wang, F. Wang, S. Salous, and J. Zhou, "Joint optimization scheme for subcarrier selection and power allocation in multicarrier dual-function radar-communication system," *IEEE Systems Journal*, vol. 15, no. 1, pp. 947–958, 2021.

[19] Y. L. Sit, C. Sturm, J. Baier, and T. Zwick, "Direction of arrival estimation using the music algorithm for a MIMO OFDM radar," in *2012 IEEE Radar Conference*, 2012, pp. 0226–0229.

[20] A. Gupta, M. Jafri, S. Srivastava, A. K. Jagannatham, and L. Hanzo, "An affine precoded superimposed pilot based mmWave MIMO-OFDM ISAC system," *IEEE Open Journal of the Communications Society*, pp. 1–1, 2024.

[21] D. P. Wipf and B. D. Rao, "Sparse Bayesian learning for basis selection," *IEEE Trans. on Signal processing*, vol. 52, no. 8, pp. 2153–2164, 2004.

[22] J. Yang, W. Li, K. Li, R. Chen, K. Zhang, D. Mao, and Y. Zhang, "Sparse bayesian learning-based multichannel radar forward-looking superresolution imaging considering grid mismatch," *IEEE Journal of Selected Topics in Applied Earth Observations and Remote Sensing*, vol. 17, pp. 14 997–15 008, 2024.

[23] A. Mehrotra, S. Srivastava, A. K. Jagannatham, and L. Hanzo, "Data-aided csi estimation using affine-precoded superimposed pilots in orthogonal time frequency space modulated mimo systems," *IEEE Transactions on Communications*, vol. 71, no. 8, pp. 4482–4498, 2023.

[24] A. M. Elbir, W. Shi, A. K. Papazafeiropoulos, P. Kourtessis, and S. Chatzinotas, "Terahertz-band channel and beam split estimation via array perturbation model," *IEEE Open Journal of the Communications Society*, vol. 4, pp. 892–907, 2023.

[25] S. D. Liyanaarachchi, T. Riihonen, C. B. Barneto, and M. Valkama, "Optimized waveforms for 5G–6G communication with sensing: Theory, simulations and experiments," *IEEE Transactions on Wireless Communications*, vol. 20, no. 12, pp. 8301–8315, 2021.

[26] E. Vargas, K. V. Mishra, R. Jacome, B. M. Sadler, and H. Arguello, "Dual-blind deconvolution for overlaid radar-communications systems," *IEEE Journal on Selected Areas in Info. Theory*, vol. 4, pp. 75–93, 2023.

[27] P. Kumari, J. Choi, N. González-Prelcic, and R. W. Heath, "IEEE 802.11 ad-based radar: An approach to joint vehicular communication-radar system," *IEEE Transactions on Vehicular Technology*, vol. 67, no. 4, pp. 3012–3027, 2017.

[28] S. H. Dokhanchi, B. S. Mysore, K. V. Mishra, and B. Ottersten, "A mmWave automotive joint radar-communications system," *IEEE Transactions on Aerospace and Electronic Systems*, vol. 55, no. 3, pp. 1241–1260, 2019.

[29] F. Liu, C. Masouros, A. P. Petropulu, H. Griffiths, and L. Hanzo, "Joint radar and communication design: Applications, state-of-the-art, and the road ahead," *IEEE Transactions on Communications*, vol. 68, no. 6, pp. 3834–3862, 2020.

[30] M. A. Islam, G. C. Alexandropoulos, and B. Smida, "Integrated sensing and communication with millimeter wave full duplex hybrid beamforming," in *ICC 2022 - IEEE International Conference on Communications*, 2022, pp. 4673–4678.

[31] S. Huang, M. Zhang, Y. Gao, and Z. Feng, "MIMO radar aided mmWave time-varying channel estimation in MU-MIMO V2X communications," *IEEE Transactions on Wireless Communications*, vol. 20, no. 11, pp. 7581–7594, 2021.

[32] Z. Gao, Z. Wan, D. Zheng, S. Tan, C. Masouros, D. W. K. Ng, and S. Chen, "Integrated sensing and communication with mmWave massive MIMO: A compressed sampling perspective," *IEEE Transactions on Wireless Communications*, vol. 22, no. 3, pp. 1745–1762, 2023.

[33] M. L. Rahman, J. A. Zhang, X. Huang, Y. J. Guo, and R. W. Heath, "Framework for a perceptive mobile network using joint communication and radar sensing," *IEEE Transactions on Aerospace and Electronic Systems*, vol. 56, no. 3, pp. 1926–1941, 2019.

[34] M. L. Rahman, P.-f. Cui, J. A. Zhang, X. Huang, Y. J. Guo, and Z. Lu, "Joint communication and radar sensing in 5G mobile network by compressive sensing," in *2019 19th International Symposium on Comm. and Information Technologies (ISCIT)*, 2019, pp. 599–604.

[35] A. Kaushik, C. Masouros, and F. Liu, "Hardware efficient joint radar-communications with hybrid precoding and RF chain optimization," in *ICC 2021-IEEE International Conference on Communications*. IEEE, 2021, pp. 1–6.

[36] L. Zheng and X. Wang, "Super-resolution delay-Doppler estimation for OFDM passive radar," *IEEE Transactions on Signal Processing*, vol. 65, no. 9, pp. 2197–2210, 2017.

[37] J. A. Zhang, F. Liu, C. Masouros, R. W. Heath, Z. Feng, L. Zheng, and A. Petropulu, "An overview of signal processing techniques for joint communication and radar sensing," *IEEE Journal of Selected Topics in Signal Processing*, vol. 15, no. 6, pp. 1295–1315, 2021.

[38] M. A. Islam, G. C. Alexandropoulos, and B. Smida, "Integrated sensing and communication with millimeter wave full duplex hybrid beamforming," in *ICC 2022 - IEEE International Conference on Communications*, 2022, pp. 4673–4678.

[39] O. A. Oumar, M. F. Siyau, and T. P. Sattar, "Comparison between music and esprit direction of arrival estimation algorithms for wireless communication systems," in *The First International Conference on Future Generation Communication Technologies*, 2012, pp. 99–103.

[40] O. E. Ayach, S. Rajagopal, S. Abu-Surra, Z. Pi, and R. W. Heath, "Spatially sparse precoding in millimeter wave MIMO systems," *IEEE Transactions on Wireless Communications*, vol. 13, no. 3, pp. 1499–1513, 2014.

[41] I. Gorodnitsky and B. Rao, "Sparse signal reconstruction from limited data using FOCUSS: a re-weighted minimum norm algorithm," *IEEE Transactions on Signal Processing*, vol. 45, no. 3, pp. 600–616, 1997.

[42] S. M. Kay, *Fundamentals of statistical signal processing: estimation theory*. Prentice-Hall, Inc., 1993.

[43] M. Li, S. Zhang, Y. Ge, Z. Li, F. Gao, and P. Fan, "STAR-RIS aided integrated sensing and communication over high mobility scenario," *IEEE Transactions on Communications*, vol. 72, no. 8, pp. 4788–4802, 2024.